AFRL-RV-PS-
TP-2014-0007
AFRL-RV-PS-
TP-2014-0007

IMPROVING AND TESTING REGIONAL ATTENUATION AND SPREADING MODELS USING WELL-CONSTRAINED SOURCE TERMS, MULTIPLE METHODS AND DATASETS
Annual Report

Mark D. Fisk, et al.

Alliant Techsystems
8560 Cinderbed Road, Suite 700
Newington, VA 22122

03 July 2013

Technical Report

AIR FORCE RESEARCH LABORATORY
Space Vehicles Directorate
3550 Aberdeen Ave SE
AIR FORCE MATERIEL COMMAND
KIRTLAND AIR FORCE BASE, NM 87117-5776

DTIC COPY

NOTICE AND SIGNATURE PAGE

Using Government drawings, specifications, or other data included in this document for any purpose other than Government procurement does not in any way obligate the U.S. Government. The fact that the Government formulated or supplied the drawings, specifications, or other data does not license the holder or any other person or corporation; or convey any rights or permission to manufacture, use, or sell any patented invention that may relate to them.

This report was cleared for public release by the 377 ABW Public Affairs Office and is available to the general public, including foreign nationals. Copies may be obtained from the Defense Technical Information Center (DTIC) (http://www.dtic.mil).

AFRL-RV-PS-TP-2014-0007 HAS BEEN REVIEWED AND IS APPROVED FOR PUBLICATION IN ACCORDANCE WITH ASSIGNED DISTRIBUTION STATEMENT.

//SIGNED//	//SIGNED//
Dr. Robert Raistrick	Glenn M. Vaughan, Colonel, USAF
Project Manager, AFRL/RVBYE	Chief, Battlespace Environment Division

This report is published in the interest of scientific and technical information exchange, and its publication does not constitute the Government's approval or disapproval of its ideas or findings.

REPORT DOCUMENTATION PAGE

Form Approved
OMB No. 0704-0188

1. REPORT DATE *(DD-MM-YYYY)*	**2. REPORT TYPE**	**3. DATES COVERED** *(From - To)*
03-07-2013	Technical Report	21 Dec 2012 – 03 Jul 2013

4. TITLE AND SUBTITLE
IMPROVING AND TESTING REGIONAL ATTENUATION AND SPREADING MODELS USING WELL-CONSTRAINED SOURCE TERMS, MULTIPLE METHODS AND DATASETS
Annual Report

5a. CONTRACT NUMBER
FA9453-13-C-0269

5b. GRANT NUMBER

5c. PROGRAM ELEMENT NUMBER
62601F

6. AUTHOR(S)
Mark D. Fisk, W. Scott Phillips, and Michael E. Pasyanos

5d. PROJECT NUMBER
1010

5e. TASK NUMBER
PPM00018848

5f. WORK UNIT NUMBER
EF122728

7. PERFORMING ORGANIZATION NAME(S) AND ADDRESS(ES)
Alliant Techsystems
8560 Cinderbed Road, Suite 700
Newington, VA 22122

8. PERFORMING ORGANIZATION REPORT NUMBER

9. SPONSORING / MONITORING AGENCY NAME(S) AND ADDRESS(ES)
Air Force Research Laboratory
Space Vehicles Directorate
3550 Aberdeen Avenue SE
Kirtland AFB, NM 87117-5776

10. SPONSOR/MONITOR'S ACRONYM(S)
AFRL/RVBYE

11. SPONSOR/MONITOR'S REPORT NUMBER(S)
AFRL-RV-PS-TP-2014-0007

12. DISTRIBUTION / AVAILABILITY STATEMENT
Approved for public release; distribution is unlimited. (377ABW-2013-0756 dtd 09 Sep 2013)

13. SUPPLEMENTARY NOTES

14. ABSTRACT

We have developed and tested methods to constrain trade-offs among source, attenuation, geometric spreading, and site effects to improve the accuracy of regional phase amplitude corrections. Our use of both coda and direct phases has corroborated a large set of source terms for Eurasia. Using distinct data and methods, we confirmed Q estimates for many paths (e.g., Fisk and Phillips, 2012, 2013a, 2013b), and delivered our results to LANL. From discrepancies, we have identified three critical ways that calibration must be improved and evaluated: (1) constrain Q near grid edges (emphasizing the Middle East), where data sampling issues are problematic for tomography, but not our method; (2) develop physically-based criteria to better control data quality for secondary phases; and (3) improve and validate Pn Q and spreading models. These issues cause large errors in P/S discrimination, illustrated for the Iranian Plateau. We are testing advanced methods to significantly improve attenuation and spreading models, site terms, and their uncertainties for Pn, Pg, Sn and Lg in Eurasia, extending to the Middle East, to corroborate and improve tomography results. We will use independent sets of coda and direct-phase measurements, and *orthogonal* methods to not only validate correction parameters, but also assess impacts on P/S discrimination. We will document and deliver the algorithms, parameter estimates, uncertainties, and evaluations. We will compare and merge our results with calibration efforts at LANL and LLNL, for incorporation in the Knowledge Base.

15. SUBJECT TERMS
Regional seismic phases, Lg coda, source terms, attenuation, geometric spreading, site effects, calibration, regional discrimination

16. SECURITY CLASSIFICATION OF:			**17. LIMITATION OF ABSTRACT**	**18. NUMBER OF PAGES**	**19a. NAME OF RESPONSIBLE PERSON**
a. REPORT	**b. ABSTRACT**	**c. THIS PAGE**			Dr. Robert Raistrick
Unclassified	Unclassified	Unclassified	Unlimited	40	**19b. TELEPHONE NUMBER** *(include area code)*

This page is intentionally left blank.

Table of Contents

List of Figures

This page is intentionally left blank.

1. INTRODUCTION

This project started six months ago. It builds upon previous efforts to establish accurate amplitude corrections for valid use of regional phases for discrimination of earthquakes and explosions, and for magnitude and explosion yield estimation. We summarize some relevant aspects of previous work in order to motivate our current R&D efforts. We then present results that we have obtained during the first six months of this project. Our team members, Dr. Scott Phillips of LANL and Dr. Michael Pasyanos of LLNL, have yet to receive their funding for this work. As such, many of the results are preliminary, but highlight our approach, the data sets, and the potential benefit.

As we have shown and discussed, procedures that simultaneously invert for source, geometric spreading, attenuation (Q), and site parameters are known to have many trade-offs (e.g., Taylor and Hartse, 1998), resulting in large errors for source and distance corrections for regional phase amplitudes, as shown by Fisk and Taylor (2006) and Fisk and Phillips (2009, 2013a). This motivated our development and application of methods to constrain the trade-offs, to improve the accuracy of the correction parameters. We have applied an empirical Green's function (EGF) approach to thousands of earthquake pairs throughout Eurasia, to cancel path and site effects, giving reliable estimates of source corner frequencies and relative moments. We used independent coda and direct phases to verify a large set of source terms (Fisk and Phillips, 2013a) that are currently being used to help constrain amplitude tomography runs. Using a subset of corroborated source terms, we then corrected the spectra of various regional phases for the corresponding source terms to estimate attenuation (Q), geometric spreading rates, and site effects. Fisk and Phillips (2013a) also showed that our estimated spreading rates for regional phases are consistent with published studies, except for long distance Pn and mantle P. As important, the spreading analysis also provides a way to establish a very consistent set of absolute scalar moments for the earthquakes. Thus, the EGF analysis provides reliable estimates of corner frequencies and relative moments; the spreading analysis brings us full circle to provide a consistent set of absolute moments.

We estimated *Q* by fitting source-corrected spectra and compared our results to tomography analysis (Fisk and Phillips, 2013b). Comparing results from independent measurements and inversion methods verifies paths with reliable Q estimates and indicates necessary improvements. We found that the Q_0 estimates from the two approaches generally agree favorably for various seismic phases, particularly for areas with good station coverage. Fisk and Phillips (2012, 2013b) describe the assumptions, approach, the overall and many detailed comparisons for various phases, showing good agreement for many paths. We also investigated large discrepancies, usually for higher frequencies, in low Q regions and/or at the edges of the tomography grid. Last, we compared our site terms to independent estimates from Lg coda tomography, showing good agreement, even for Pg and Pn, at many stations, as well as some significant differences. By comparing results of the distinct methods, we have identified three critical ways that *Q* and spreading models must be improved and tested. First, given that some very important areas are near grid edges, where tomography results are known to have significant errors, we need to assess their impact on discrimination and redress the problems. Second, data quality has a direct impact on calibration. Simple signal-to-noise ratios (SNR) using pre-Pn and/or pre-phase noise measures do not exclude sufficient bad data, while retaining a majority of good data, particularly for secondary phases that are in the coda of preceding phases. Third, Pg is typically more stable than Pn, but there are only a fraction of Pg observations compared to Pn, which

has significant calibration issues. We have shown order-of-magnitude errors due to these issues that directly impact P/S discrimination results. Rectifying them and incorporating the enhancements in calibration deliveries are essential. The following describes each of these in more detail.

2. BACKGROUND AND MOTIVATION

To better see where *Q* estimates from spectral fitting versus tomography differ, we differenced *Q* grids, given in percentage, for various phases and frequencies. For example, Figures 1 and 2 show the percent differences of Sn *Q* at 1 Hz and 5 Hz respectively. The map for 1 Hz shows some modest differences. The map for 5 Hz indicates differences as large as 200% in some areas, generally to the west and south of most IRIS stations, systematically biased higher for tomography. We examined numerous interesting discrepancies and showed that many can be reconciled. Several paths are depicted in the lower map, corresponding to significant differences that we have examined in detail.

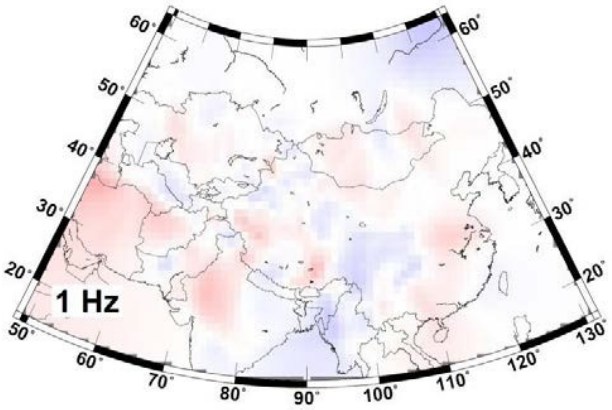

Figure 1. Percent difference of Sn Q estimates from tomography and fitting source-corrected spectra at 1 Hz. *The color scale is the same as in Figure 2.*

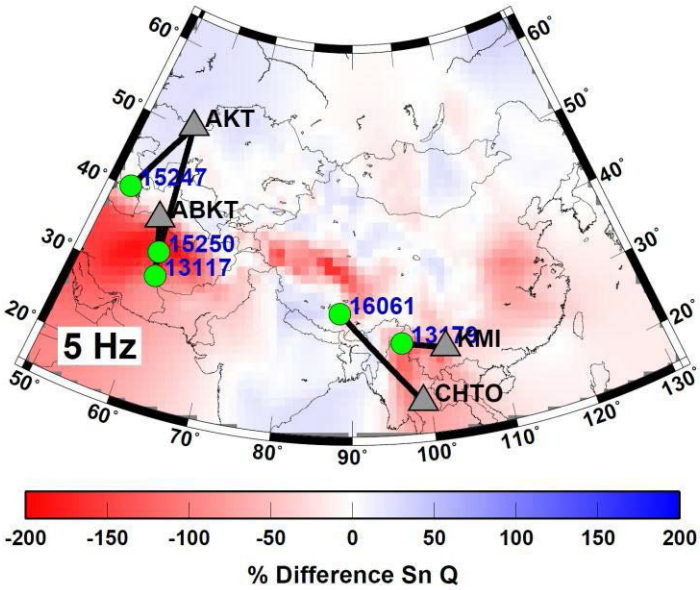

Figure 2. Percent difference of Sn Q estimates from tomography and fitting source-corrected spectra at 5 Hz. *Detailed Q results are presented for the paths shown.*

2.1. Tomography Edge Effects and Implications for P/S Discrimination

First, a serious issue we have noted previously (e.g., Fisk and Phillips, 2011, 2012, 2013b) is that amplitude tomography results can have large errors near the edges, where there are insufficient crossing ray paths to resolve various physical effects. In fact, many of the clearest discrepancies between the Q grids from fitting source-corrected spectra and amplitude tomography are near the tomography grid boundary. Now that we have estimated *Q* for regional S and P phases, and given that some key areas are near grid edges, it is interesting to assess how those errors impact P/S discrimination. We have processed some clusters in Iran, including those labeled in Figures 1 and 2 and the map in Figure 3, which also compares Pn or Pg (left) and Lg (right) *Q* results for various paths at the western edge of the tomography grid. The upper right plot shows that there are some very good Q comparisons, typically for higher Q paths with better station coverage, in this case for the path from event 15247 to station AKT (Aktyubinsk, Kazakhstan). Discrepancies are progressively worse for lower *Q* and poor ray-path sampling. In fact, the bottom right plot of Figure 3 is one of the largest γ discrepancies we found for Lg. Note that the lower bands of the tomography results (green circles) in these plots agree with the source-corrected spectra, but deviate higher for higher bands that are important for P/S discrimination, due to worse sampling (fewer crossing paths). Our estimates of source and Q effects from spectral fitting do not depend on sampling issues (e.g., crossing ray paths); hence, they can be used to improve amplitude tomography results at grid edges. A key scientific question is how these errors affect P/S discrimination.

The left plot of Figure 4 shows Pn/Lg and Pn/Sn ratios at AKT for event 15250. The green and red curves correspond to using our Q corrections, and those from tomography, respectively. Note that the corresponding tomography *Q* predictions (cf. middle plots of Figure 3) are both higher than the source-corrected Lg and Pn spectra at high frequencies, but the errors are comparable and largely cancel, giving corrected P/S ratios near one, appropriate for earthquakes. The right plot of Figure 4 shows that the errors do not cancel for any of the P/S ratios using tomography *Q* corrections from either Phillips et al. (2009, red curves) or Pasyanos et al. (2009, magenta curves), leading to P/S ratios as high as 10-20 at higher frequencies, i.e., very explosion-like. For comparison, the corrected Pn/Lg mean for Nevada Test Site explosions is 5.5 for the 4-6 Hz band, and 5.8 for the 6-8 Hz band (Fisk et al., 2010), as depicted by the horizontal black lines in the lower plot. We have thoroughly investigated possible explanations for the high P/S ratios, when using the tomography *Q* corrections. (Note that we have also found cases for which Pn/Sn or Pn/Lg spectral ratios, corrected by tomography Q results, are an order of magnitude too low.) Sparing the details here, we have excluded (1) measurement differences, (2) corner frequency effects, (3) very different site effects at ABKT for Pn and Pg, than for Sn and Lg, and (4) frequency-dependent spreading. The problem is the well-known fact that tomography is unstable in areas with limited or no crossing ray paths, and depends of the number of observations, crossing ray paths, and SNR for various phases. To avoid false alarms, large uncertainties can be assigned to tomography *Q* estimates near grid boundaries. However, given these errors and reasonable uncertainties, all events in this important area would be *undetermined*. Given the investment in tomography work, this problem must be addressed, providing *Q* estimates that are verified by multiple methods and datasets.

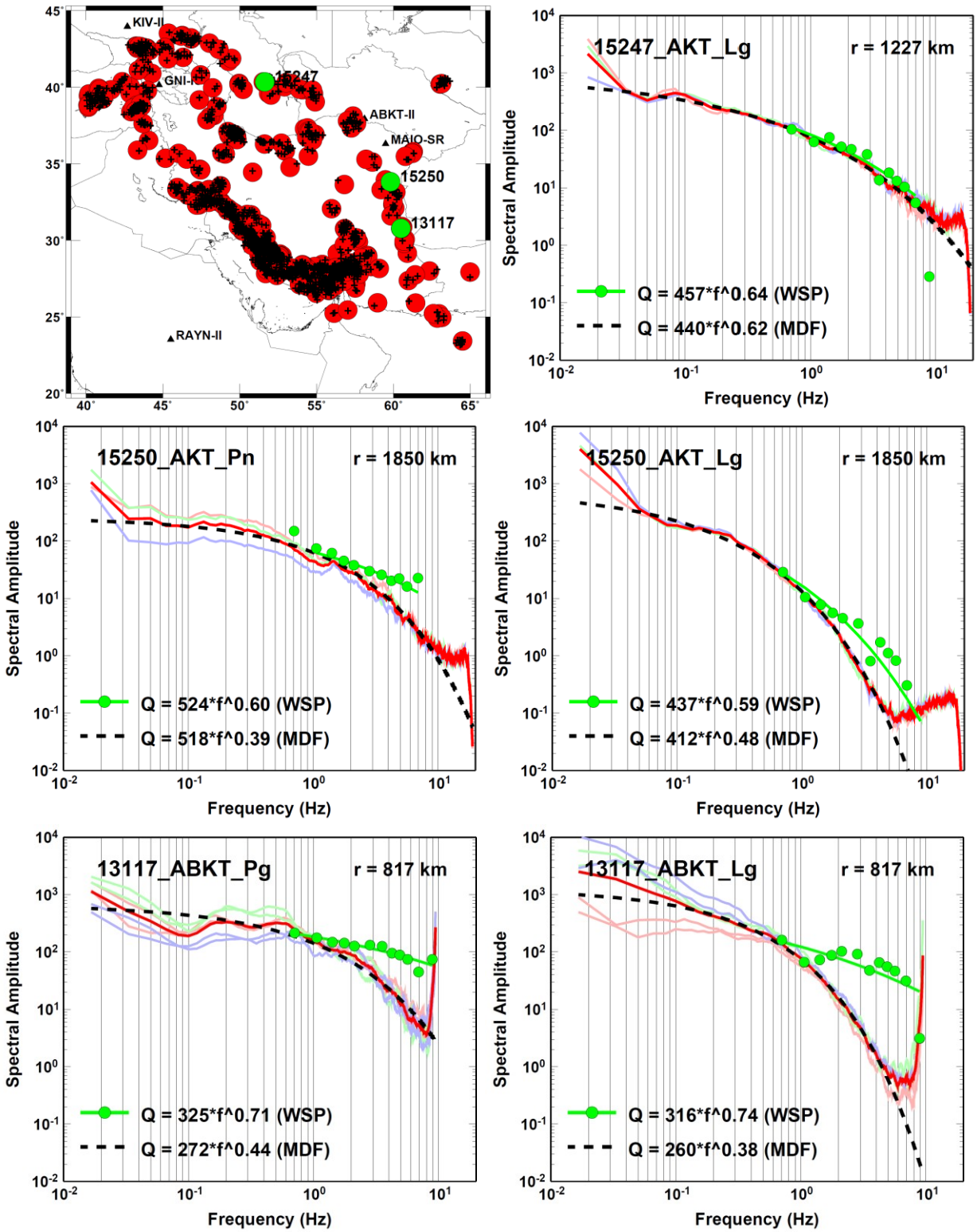

Figure 3. Comparisons of Pn or Pg (left) and Lg (right) spectral fits to tomography results for three clusters in Iran (green circles in top left map).

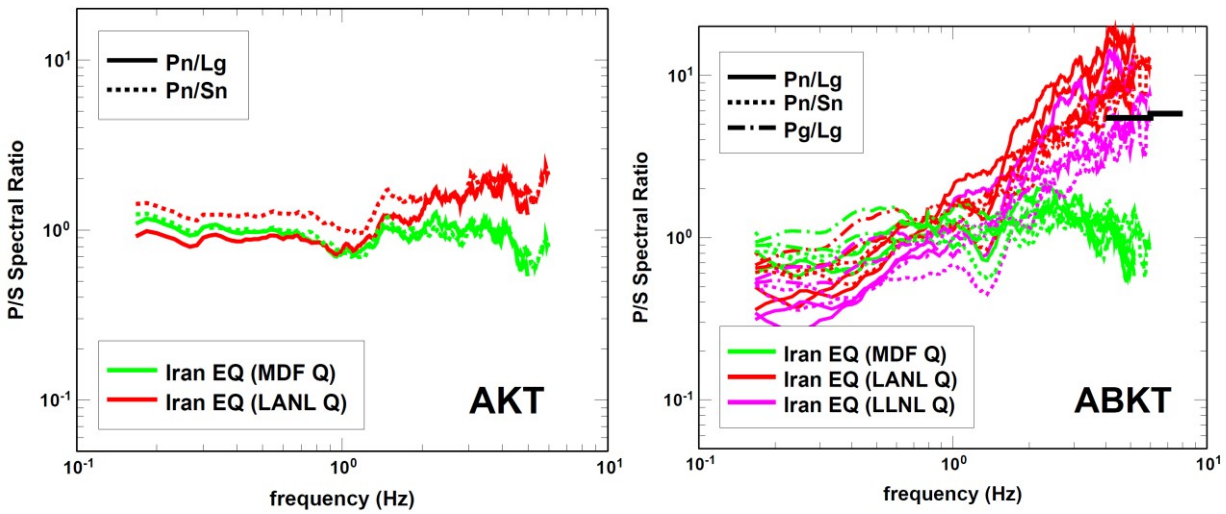

Figure 4. P/S spectral ratios at AKT for event 15250 (left) and ABKT for event 13117 (right), using Q corrections from fitting source-corrected spectra (labeled MDF), and from tomography by LANL and LLNL (see legends).

2.2. Data Quality Control

Second, data quality directly impacts calibration. Quality control (QC) is a very important and non-trivial aspect of any seismic data processing. SNR thresholds are typically used. However, there are many ways that bad data can pass an SNR test and good data can fail. For example, clipped data have spurious high-frequency signals that can easily pass the test. Alternatively, aberrant signals in the noise window can cause good signals to be rejected. This is especially complicated for secondary phases because pre-phase noise measurements include preceding phases. For example, a valid Lg signal may be rejected, depending on the threshold, because the noise window includes Sn. Alternatively, using pre-Pn noise can accept Sn or Lg signals that are actually coda of P phases. There is no simple way to automate noise windows and SNR thresholds that avoids all such complications. Correcting amplitudes for "noise" is fraught with the same problems. We used a straightforward (semi-automated) approach to find low and high frequencies of a spectrum where it departs from *normal* physical behavior, i.e., inflections at frequencies where noise starts biasing the spectrum high from expected decay (cf. Figure 5). Although not all cases are easy, examination and fitting of thousands of spectra suggests that such frequency ranges can be found for most. Further work is needed to implement and test fully automatic criteria to supplement the SNR tests, and assess improvements to tomography results, particularly for low Q paths.

Figure 5 (left) illustrates a prevalent problem for a relatively low-Q path from an earthquake in Tibet to station CHTO in Thailand (cf. Figures 1 and 2), in which tomography *Q(f)* results agree with the source-corrected spectrum for lower bands, but deviate significantly higher in bands above 3 Hz, for this case, due to noise effects. (As shown below, over-estimating *Q* for regional S phases biases P/S ratios high, i.e., making earthquakes seem more explosion-like.) The signal-to-noise criteria used for tomography (pre-Pn SNR>2 and pre-phase SNR>1.2) were intentionally lax, to utilize more data. If SNR tests are too stringent, data sampling issues can arise. Excluding the tomography *Q(f)* values in higher bands, Figure 5 (right) shows that the Q_0 and γ estimates now

agree. Many seismic amplitudes, especially at higher frequencies for low-*Q* paths, are corrupted by noise. Results of our distinct methods can be reconciled to corroborate the *Q* estimates. Note that our spectral fit (black curve) in Figure 5 is automatic, including determining the frequency range of the fit. The inflection at about 2 Hz, where noise starts biasing the spectrum high from expected decay, is usually straightforward to find. Although not all cases are easy, examination and fitting of thousands of spectra suggests that such valid frequency ranges can be found for most, which could be used to improve data quality before performing amplitude tomography. In a subsequent section, we will show that the frequency range of useful regional signals is even easier to determine when using ratios of P/S spectra.

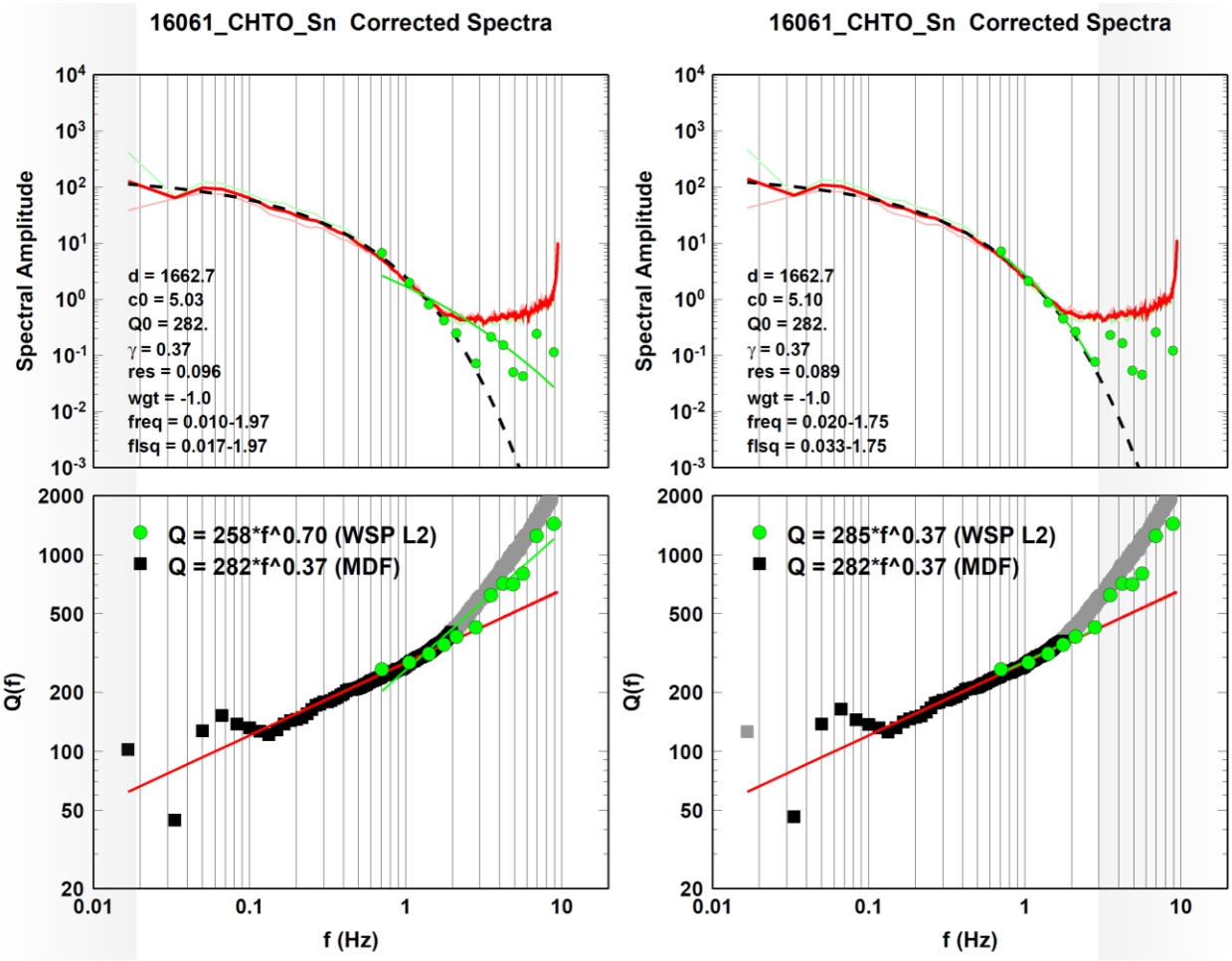

Figure 5. Comparisons of Sn Q results for an earthquake in Tibet to station CHTO, including all tomography Q bands (left) and excluding bands greater than 3 Hz (right).

2.3. Improved Pn Q and Spreading Models

Calibration of Q and geometric spreading models for Pn is generally much more complicated and challenging than for Lg and Sn, but equally important for valid application of P/S discriminants to broad areas. We have reviewed Pn (checking picks, data quality, and fits of source-corrected spectra) for 2672 paths. Pn spectra for distances less than ~300 km are complicated by short time

windows and ones that measure noise or Pg, depending on actual versus predicted arrival times. Pn spectra are the most variable and most time consuming to review. Although Pg/Lg typically has the lowest variance of various P/S discriminants, Pn/Lg and Pn/Sn discriminate better for calibrated areas (e.g., Walter et al., 1995; Fisk et al., 1996; Bottone et al., 2002). In addition, for broad area monitoring, the ratio of Pg to Pn observations is roughly 1:4 (e.g., 714 versus 2672) for the same set of events. This is why it is so important to obtain good calibration for Pn. The green circles in Figure 6 are Pn spectral fit constants versus distance for 2237 reviewed paths, so far. Fitting Eq. (8) to all points out to 2000 km gives a standard deviation of $\sigma = 0.37$. Fitting data out to 1500 km, gives $\eta = 1.06$ and $\sigma = 0.28$. For farther distances, the spectral constants are considerably higher, on average, than the black curve. We have investigated this carefully, using a subset of large earthquakes, and find that this is not a noise effect. It is a physical departure from constant power-law spreading for Pn, presumably due to upper mantle triplication, sphericity, and other complicated Pn propagation effects (noted by, e.g., Yang et al., 2007; Yang, 2011; Avants et al., 2011). We have also tested quadratic (blue curve in Figure 6) and piecewise regression fits. Dr. Phillips has b

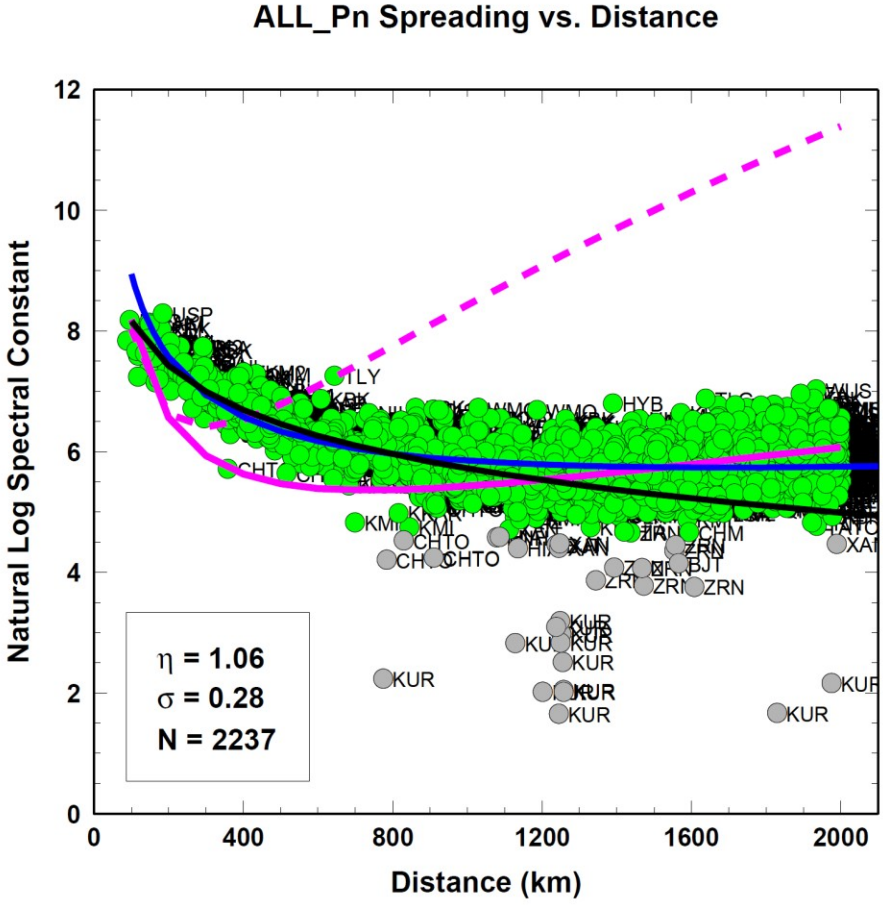

Figure 6. Pn spreading results for 2237 paths. *The black curve is the regression fit out to 1500 km. The blue curve is a quadratic fit out to 2000 km. Magenta curves are the spreading model of Yang (2011) for frequencies of 1 Hz (solid) and 10 Hz (dashed).*

The magenta curves in Figure 6 show the Pn spreading predictions of Yang (2011) [Y2011] for 1 Hz and 10 Hz. In deriving the model, he (1) applied generic Brune (1970) source corrections, using MDAC scaling relations of moment and corner frequency to mb, (2) corrected the amplitudes by

the simulations of Yang et al. (2007) [Y2007], using a homogeneous, two-layer, spherical model, (3) estimated an average *Q* for Eurasia from those corrected data, (4) applied that *Q* correction, excluding the Y2007 spreading correction, and (5) then fit 6 or 12 parameters to represent the resulting frequency and distance behavior. Comparing spreading models with or without frequency dependence is complicated, but note that the magenta curves predict elastic 10-Hz Pn amplitudes at 1500 km a factor of 36 larger than at 300 km, and 73 times larger than 1-Hz Pn at 1500 km. Y2007 explain this as whispering gallery effects and argue that their spreading model leads to reasonable Pn *Q*. This assumes that the source corrections he used are valid. However, as we have shown (cf. Fisk and Phillips, 2013a), the XP99 (used by Y2007) and MDAC (used by Y2011) source scaling relations both have significant errors. Using our large set of verified source terms, we can directly test whether Y2011, or any other, spreading corrections, really yield reasonable Pn *Q*. For example, Figure 7 compares Pn Q results for paths from the Lop Nor Test Site (LNTS) to stations AAK and TLY, indicating the range of agreement, as well as the need for improvements. The plots also show the Pn spreading predictions of Y2011 versus frequency. For AAK (at a distance of 1158 km), if we apply that correction prior to fitting for *Q*, it gives $Q(f) = 68\ f^{0.67}$, very inconsistent with the source-corrected spectral behavior and the *Q* estimates in Figure 7. We have discussed these results with Dr. David Yang and Prof. Thorne Lay.

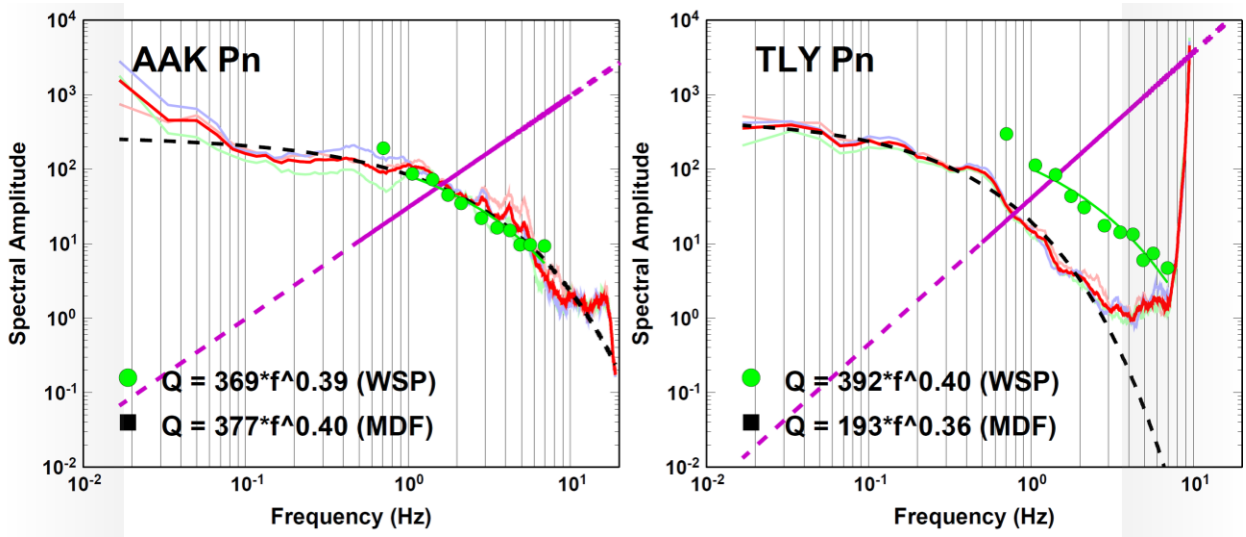

Figure 7. Source-corrected Pn spectra, Q model fits, and tomography results at AAK and TLY for an earthquake at LNTS. *The magenta lines are Y2011 Pn spreading predictions.*

To understand the physical issues, the standard model of Eq. (1), used by countless researchers, assigns all frequency-dependent distance effects to *Q(f)* because data alone cannot separately estimate a frequency-dependent spreading term. Y2007 splits the distance terms into sphericity effects, simulated for a homogeneous model, and a definition of *Q(f)* that includes anelastic and all unmodeled elastic scattering effects. (The simulations are also embedded in the semi-empirical Y2011 spreading model.) Avants et al. (2011) note that fully inclusive spreading would consider elastic scattering in a heterogeneous earth. They find that mantle lid velocity gradients systematically alter frequency-dependent spreading from that found for constant velocity, and random lateral heterogeneities in the uppermost mantle give Pn spreading approaching power-law behavior as the RMS strength of heterogeneity increases. (The "spreading" simulations of Y2007 do not treat these important elastic scattering effects.) So the

distance effects are split differently, but neither has a purely anelastic definition of *Q(f)*, nor gives better corrections or physical interpretation, until realistic velocity gradients and heterogeneities can be modeled on large 3D scales. Lay and Yang have proposed research that should improve scientific understanding on this very important problem. The hardest part will be to validate the model simulations, given empirical limitations to resolve these effects.

These results indicate the importance of Pn for P/S discrimination, as well as the need to improve existing Pn spreading and *Q* models. Using reviewed data with well constrained source terms, the Pn spectral fit constants (green circles in Figure 6) clearly depart from constant power-law spreading, showing the need for a better model. As illustrated for Lop Nor, Pn *Q* estimates are verified for many paths, but there are also many large discrepancies (e.g., for TLY), much more so for areas lacking good ray-path sampling. Previous Pn tomography runs at LANL obtained some very high, or even negative, *Q* estimates (i.e., predicting increasing amplitudes with increasing distance). A Pn spreading model that accounts for the rise at far regional distances (cf. Figure 6) due to, e.g., triplication effects, may remedy unphysical Pn *Q* values from amplitude tomography. Calibration of Pn is a very difficult problem because of its variability from a host of complicated effects. However, more accurate, robust, and compact Pn *Q* and spreading models are attainable than currently exist.

3. RESEACH ACCOMPLISHED

Given this background and motivation for our existing work, we have been proceeding on three main fronts, which are largely driven by the extant availability of datasets to this point, because our partners at LANL and LLNL have yet to receive their funding. Thus, in the first quarter of this effort, we focused on applying our approach to IRIS data for the Iranian Plateau to estimate source terms and Q parameters. Subsequently, Dr. Phillips provided openly-available data from the University of Tehran and, later, from the International Institute of Earthquake Engineering and Seismology (IIEES). The former dataset has more data quality issues and many of the instrument responses are currently unreliable. We were aware of this all along, and discussed strategies in our proposal to still make valuable use of these data. The IIEES dataset does have reliable responses and fewer data quality problems, availing application of our full complement of analyses. We describe each of these studies here, with the clear caveat that these are very preliminary results at this stage in the project.

3.1. EGF and Q Analyses of IRIS Data for the Iranian Plateau

Extending our EGF analysis of IRIS data to the clusters shown in the map of Figure 3, Figure 8 (left) shows the relative spectra for one pair in a cluster in northern Iran, using data from ABKT and KKAR. Despite considerable spectral variability, due to smaller events occurring shortly after the main shock and data from only two stations, the results for direct phases and coda are reasonably consistent. The right plot shows the scaling of source parameters for four earthquake pairs. Figure 9 shows the location of the cluster (main shock) and compares Lg and Pn Q_0 results for various paths. Figure 10 shows the source-corrected spectra and compares Q estimates to those from amplitude tomography for paths to stations ABKAR and ABKT. Pn Q_0 results compare favorably, although tomography γ estimates (Q estimates at higher frequencies) are biased higher. The most notable Q differences are for Sn and Lg along the path to ABKT, as we saw for clusters in southern Iran that we processed previously.

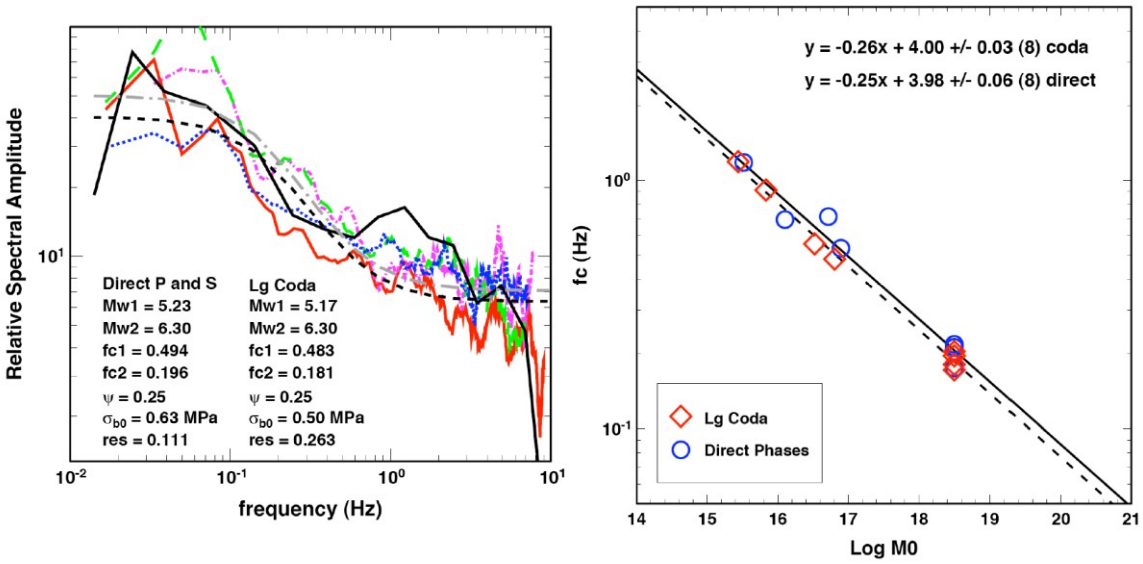

Figure 8. (Left) Relative spectra and source model fits for one earthquake pair in northern Iran. (Right) Estimates of corner frequencies versus log moments for four earthquake pairs.

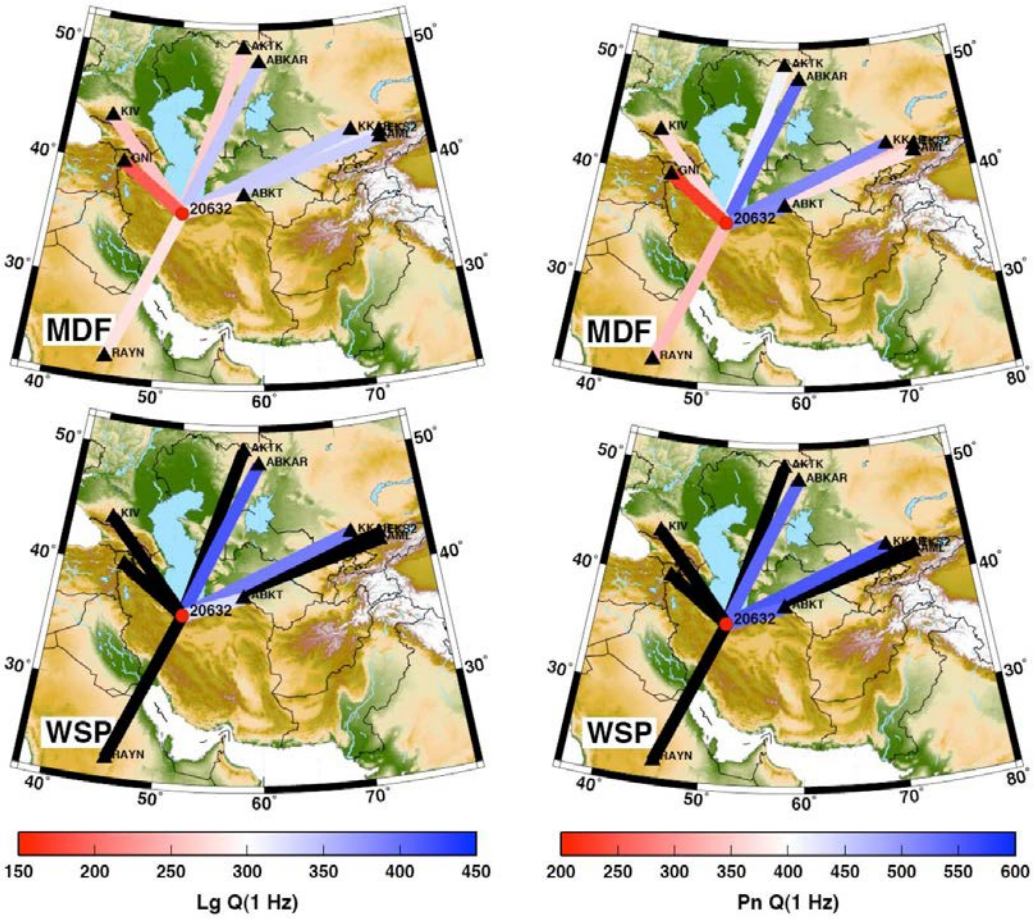

Figure 9. Comparisons of Q_0 estimates for Lg (left) and Pn (right) from fitting source-corrected spectra (top) and tomography (bottom). *Black rays indicate no tomography results, at present.*

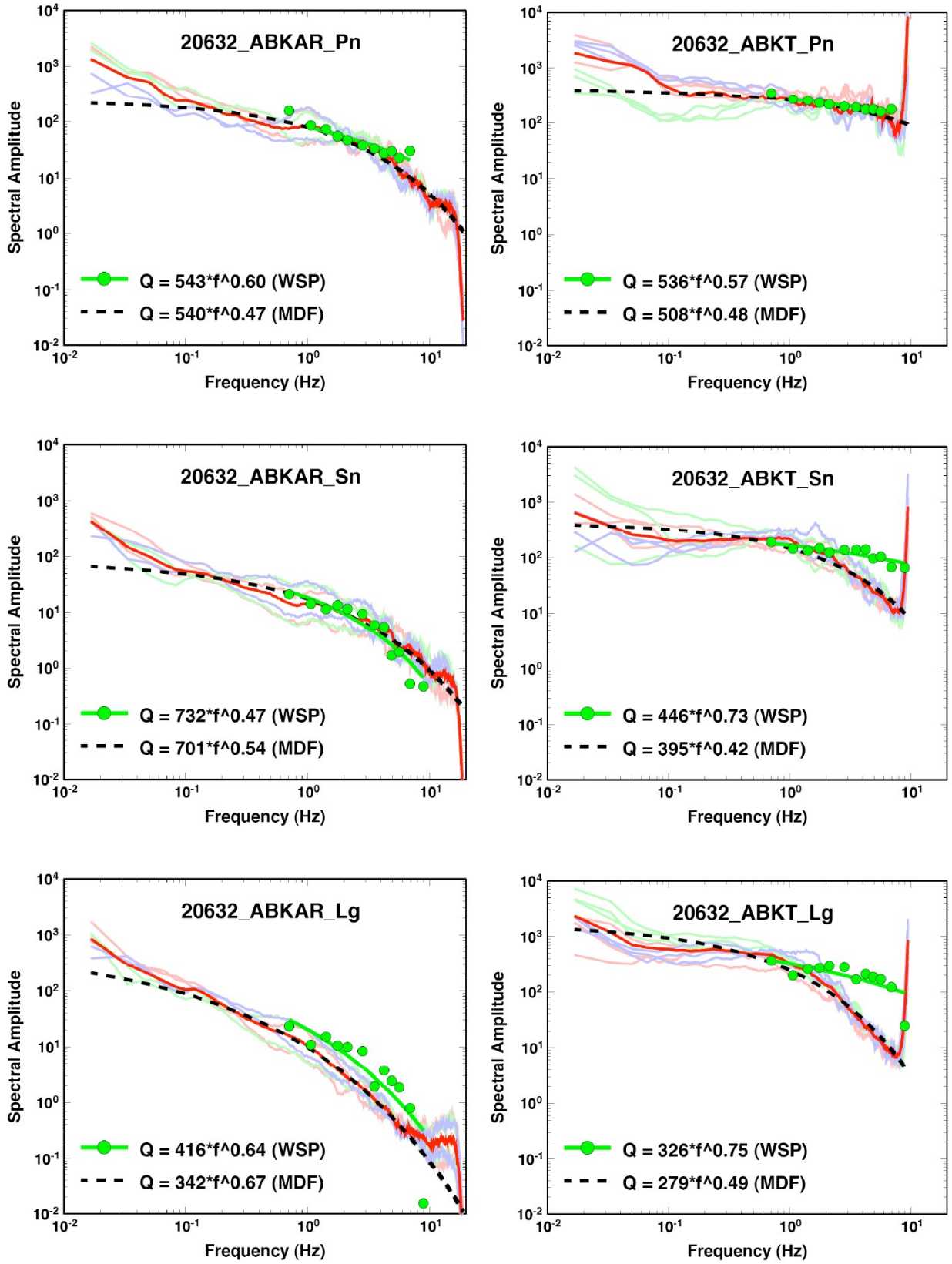

Figure 10. Source-corrected spectra and Q estimates for Pn, Sn, and Lg at ABKAR and ABKT.

Figure 11 shows the fit constants of the source-corrected spectra versus distance for the various phases, as compared to the geometric spreading (gray) curves for Eurasia that we derived previously. In general, the spreading results are consistent, although we found that the PDE Mw 6.3 for the main shock is about 0.1 m.u. too high. These source results can be used to calibrate paths in northern Iran to any recording station, including those in country.

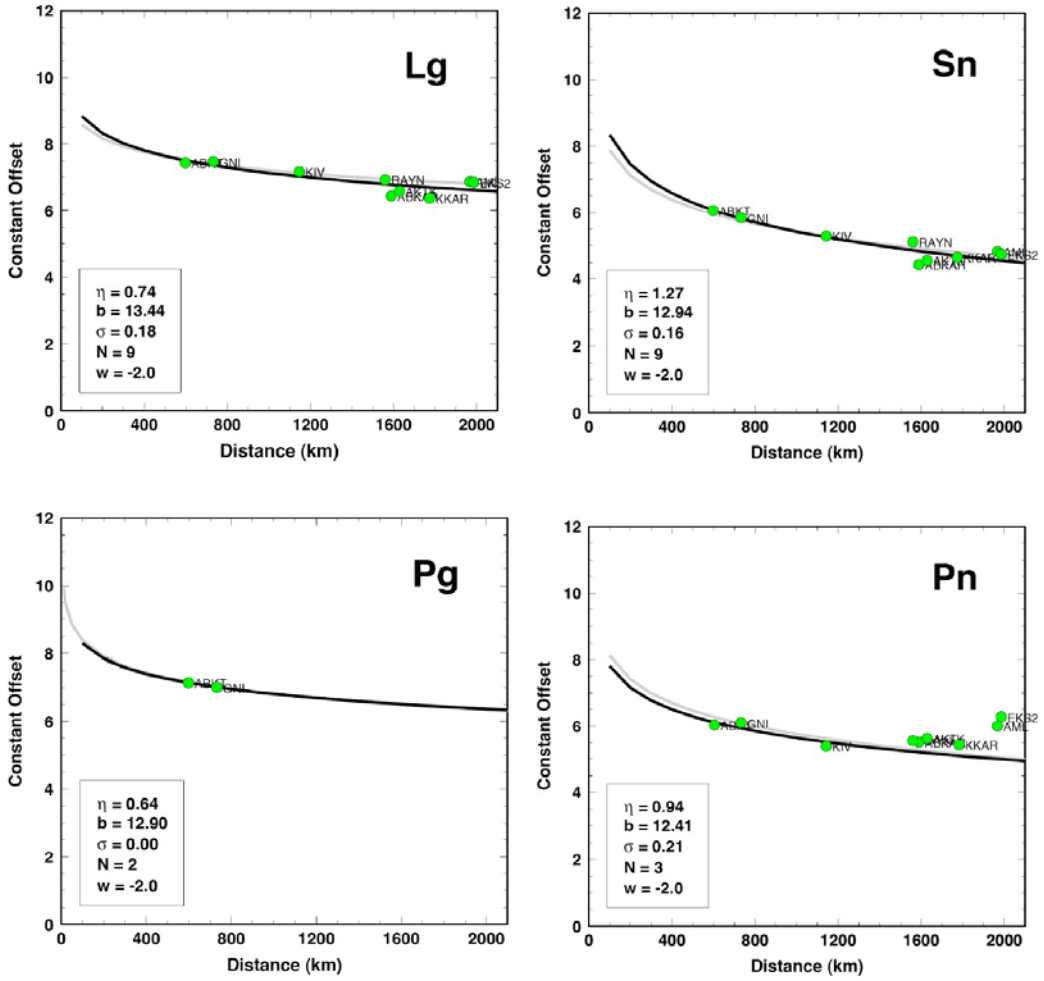

Figure 11. Source-corrected spectral constants versus distance for various regional phases, their regressions (black curves), and geometric spreading results for Eurasia (gray curves).

Figure 12 compares some representative S/P ratios (Lg/Pn, Sn/Pn, Lg/Pg) for the main shock to predictions based on tomography (dotted curves) and fits of source-corrected spectra (stippled). The solid curves represent fits of a new model to the spectral ratios; the constant term (*a* in the legends) is equivalent to the difference of frequency-independent geometric spreading for the S and P waves. The *b* and *c* coefficients represent differential attenuation effects. Predominantly, S waves attenuate more rapidly than P waves, but this is not always the case. For example, Sn and Pn have very small differences in attenuation effects for the path to ABKAR. In some cases the tomography results agree reasonably well with the S/P ratios. However, note that by performing the inversions separately for various P and S phases, the errors can be opposite, causing large accumulated errors in either over- or under-predicting S/P ratios.

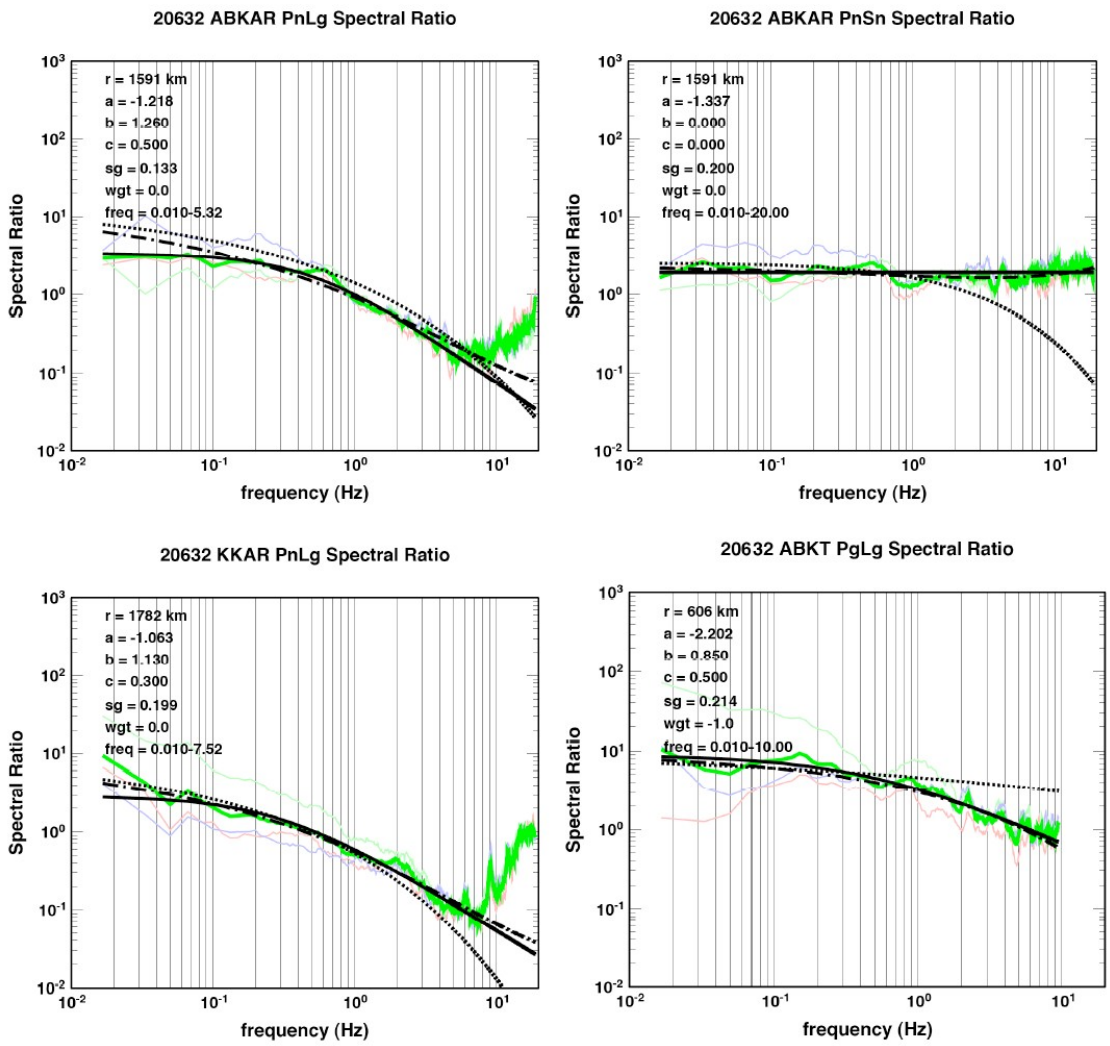

Figure 12. Examples of S/P spectral ratios. *Dotted, stippled, and solid curves are predictions from tomography, fitting source-corrected spectra, and direct fits using a new model.*

As noted in our proposal, a significant fraction of in-country data do not have reliable responses. As one option, we discussed inverting S/P ratios, rather than raw amplitudes, to be used as constraints for tomography. In preparation for this, we compared various S/P ratios to Q predictions. (Below, we present some local data that we recently acquired and processed.) Figure 13 shows the corresponding Lg/Pn spectral ratios, along with Q predictions from spectral fitting (dashed) and tomography (dotted), and direct fits (solid curves) for two paths, illustrating two common observations. First, the actual S/P ratios do not have the curvature predicted by exponential attenuation functions. Rather, they are often fairly flat at low frequency and then decay like a power law of frequency, not an exponential of a frequency-dependent power law. In fact, the simple three-parameter model (compared to six parameters, treating spreading and Q independently for each phase), illustrated by the solid curves, provides a better representation of the observed functional form. A possible physical interpretation is that elastic scattering effects may be more responsible for differential frequency-dependent S/P behavior than anelastic attenuation that is represented by exponentially decaying terms, perhaps corroborating findings by Morozov (2008) and Morozov et al. (2008). Second, the S/P spectral ratios show clear minima, corresponding to the maximum

frequency of useful Lg signals (discussed below). Figure 14 shows fit coefficients (slope and intercept parameters) for Pn/Sn and Pn/Lg spectral ratios for paths from LNTS to regional stations. The intercepts are related to what is defined as frequency-independent spreading in the *standard* model. The slopes (circles) depend on the relative S and P attenuation (related to γ values). Not surprisingly, the intercepts for Pn/Sn do not exhibit a trend with distance because Pn and Sn spreading coefficients are both about 1.1. This is not the case for Pn/Lg (right plot) because the Lg spreading rate is about 0.6. As we showed previously (Fisk and Phillips, 2012, 2013a), the Pn spectral constants deviate higher at far regional distances due to P-wave triplication effects.

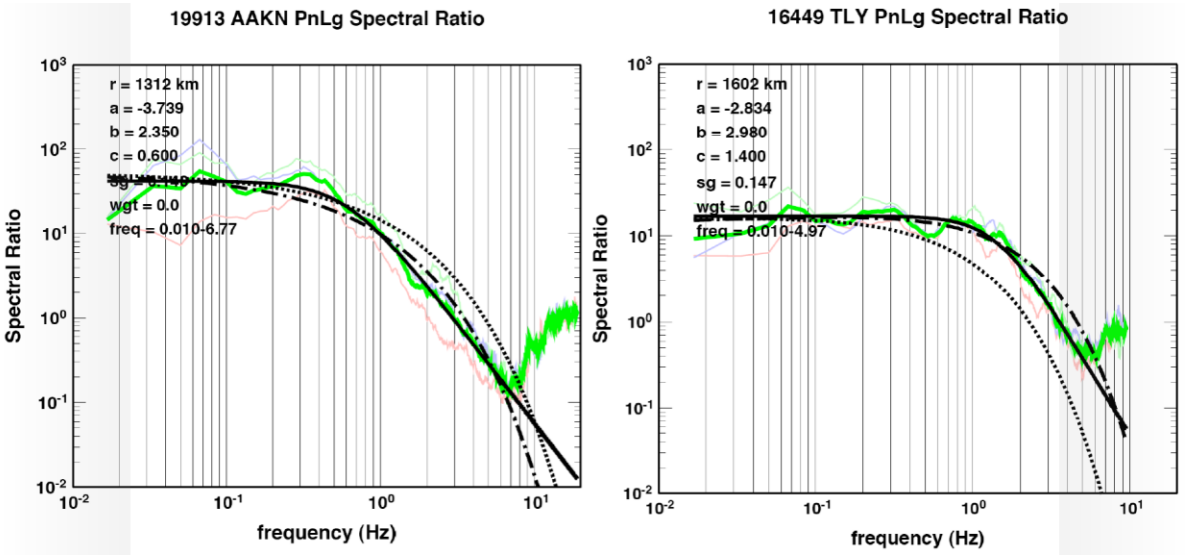

Figure 13. Lg/Pn spectral ratios and comparisons to Q predictions for two paths, (left) from southwestern Siberia to KNET station AAK and (right) from LNTS to station TLY.

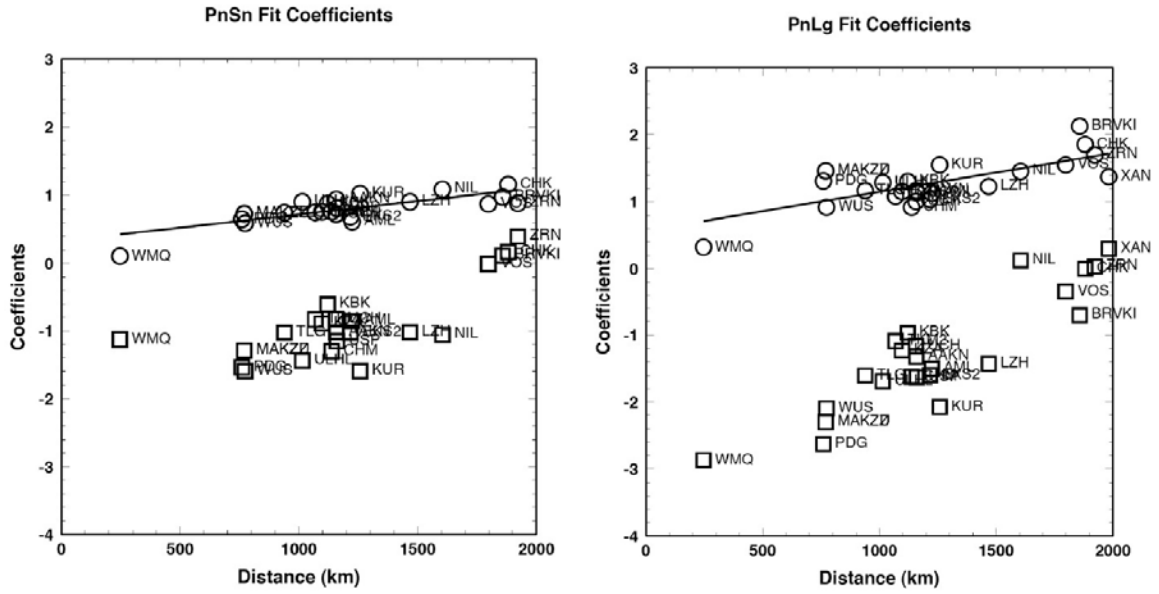

Figure 14. Slopes (circles) and intercepts (squares) of Pn/Sn (left) and Pn/Lg (right) spectral ratios for regional paths from LNTS.

Related to data quality control, Figures 12 and 13 illustrate that the maximum frequency (Fmax), corresponding to the S/P spectral minimum, is usually easy to determine, more so than for the individual source-corrected spectra. Because S waves usually attenuate faster than P waves along a given path, the minimum usually corresponds to the maximum frequency for the S wave. The Kazakh Platform is an exception, where Pn and Sn attenuate comparably. Determining the useful frequency range of secondary phases is of particular interest to calibration and monitoring. Figure 15 shows Fmax of Lg/Pn versus distance for paths from an Mw 5.5 earthquake at LNTS to regional stations. Note that WMQ and MAKZ stations (IU and KZ networks) have Nyquist frequencies of 10 Hz, thus not representing the true bandwidth of the signal. As expected, the maximum frequency for LSA is very low, corresponding to very low Lg Q for that path through the Tibetan Plateau. We have compiled such results for a larger, preliminary set of data, sampled throughout Eurasia. From this information, and accounting for Nyquist saturation issues, we can begin to quantify the maximum frequency as a function of magnitude, epicentral distance, and Q.

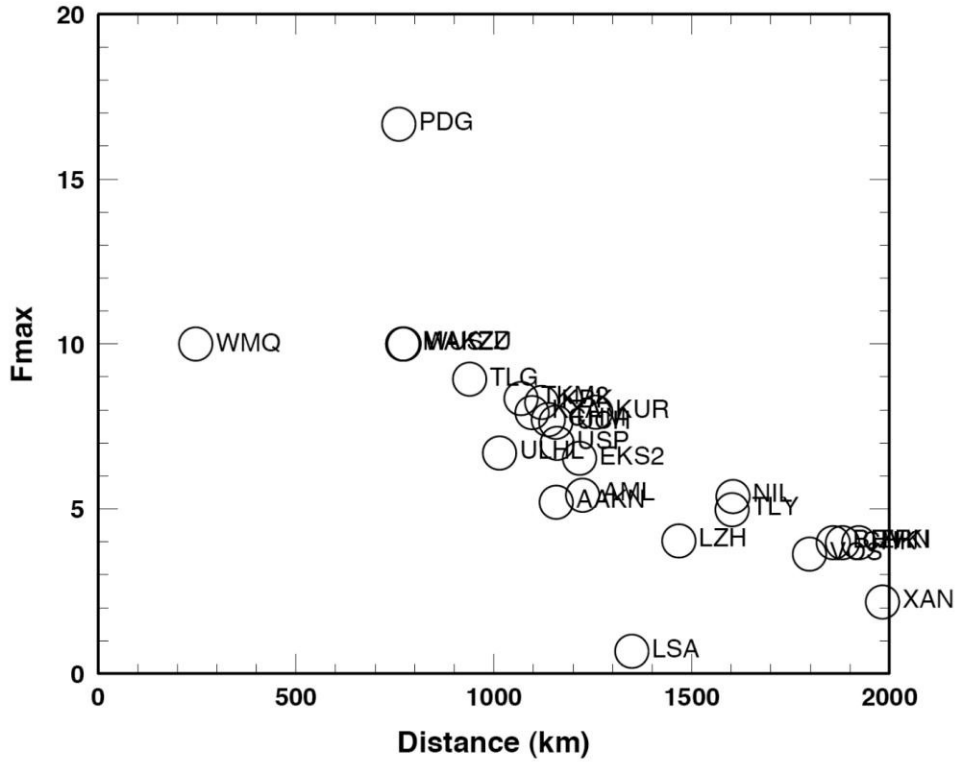

Figure 15. Maximum frequencies of Pn/Lg spectral ratios versus distance for regional paths from LNTS, showing a clear trend with distance. *Some results are truncated due to a Nyquist of 10 Hz. The bandwidth for LSA is particularly low, as expected, because Lg Q is quite low.*

Figures 16-18 geographically depict a subset of Pn/Lg, Pg/Lg and Pn/Sn results for the Iranian Plateau, showing the values of the P/S ratios for various paths, limited to those with Fmax greater than to the frequency plotted. These events are mb>5, so the coverage for a given frequency may be considered an upper bound. The progression of plots in Figure 16 indicates that Lg attenuates rapidly at higher frequencies, except for shorter paths and/or high-quality propagation to, e.g., station AKTK. Figure 17 highlights a point we have made previously, i.e.,

that the number of Pg observations is considerably less than for Pn. Pn/Sn (cf. Figure 18) has the most observations at higher frequencies, relevant to the application rate of various regional discriminants. These data, including clear indication of bandwidth and augmented with in-country data, when available, can be used to provide excellent calibration of this region.

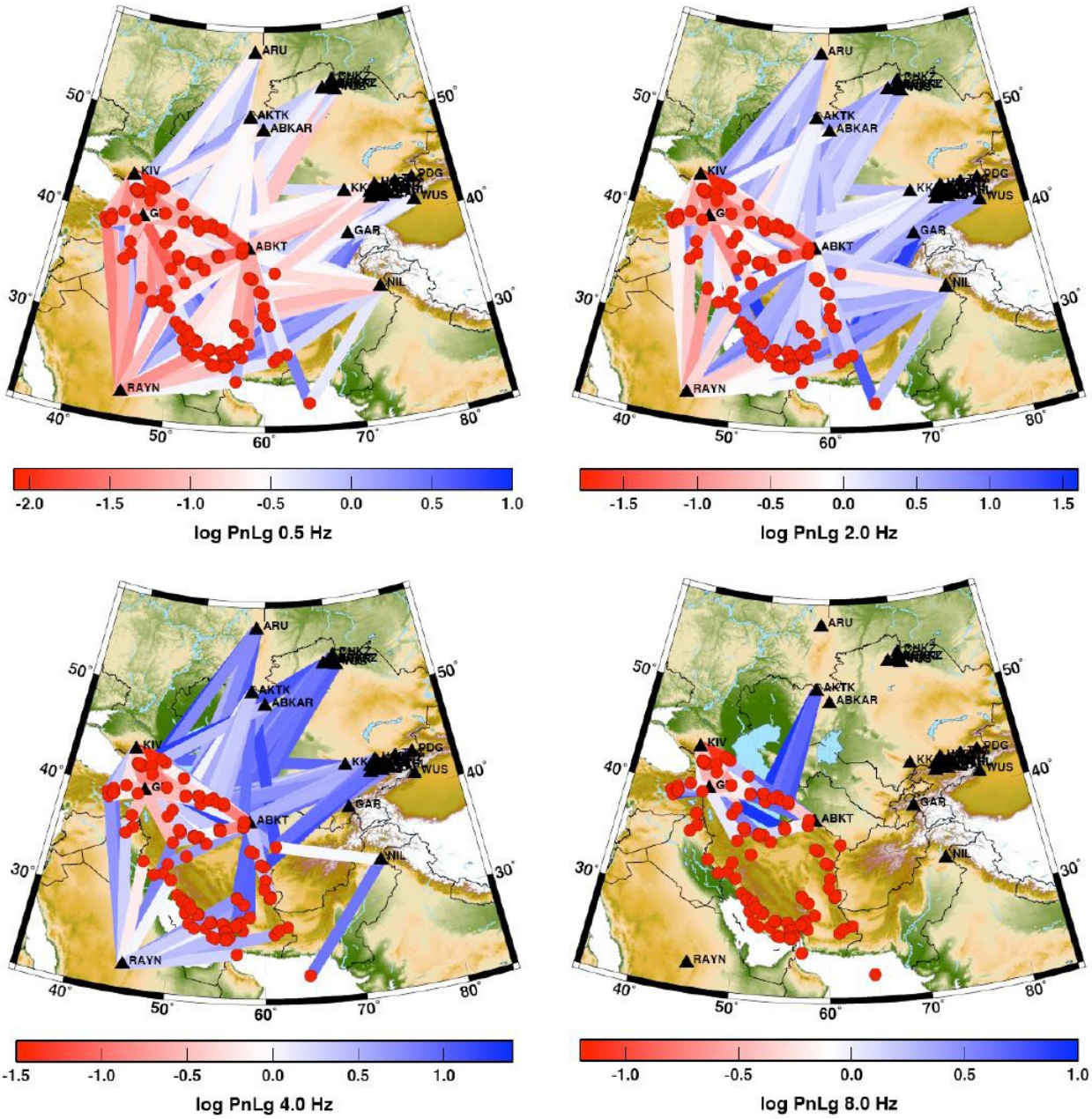

Figure 16. Raw log Pn/Lg values along various paths for four frequencies, plotted only if the maximum frequency of the Pn/Lg spectral ratio is greater than or equal to the selected frequency (0.5, 2.0, 4.0, or 8.0 Hz).

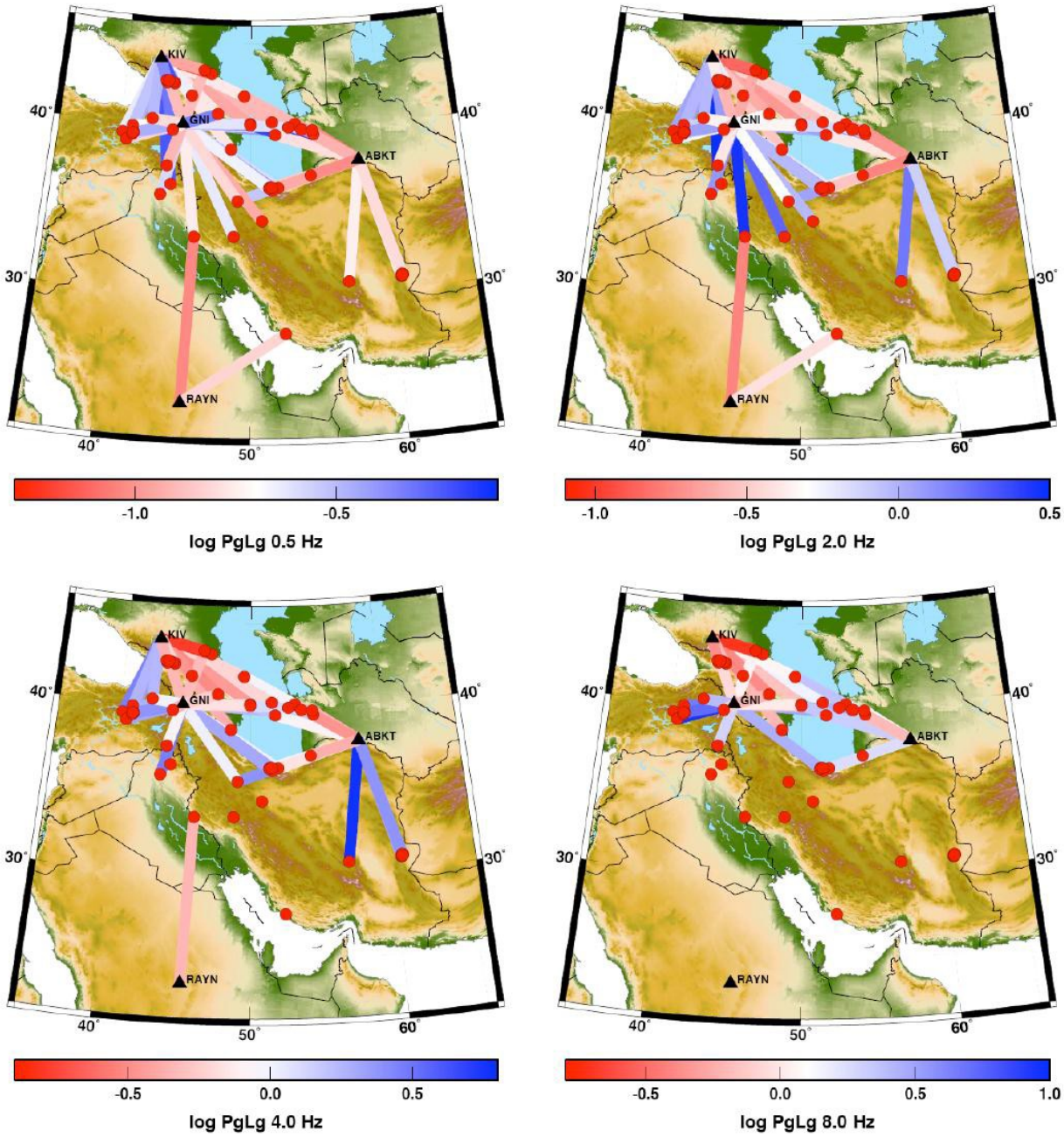

Figure 17. Similar to Figure 16, but for Pg/Lg.

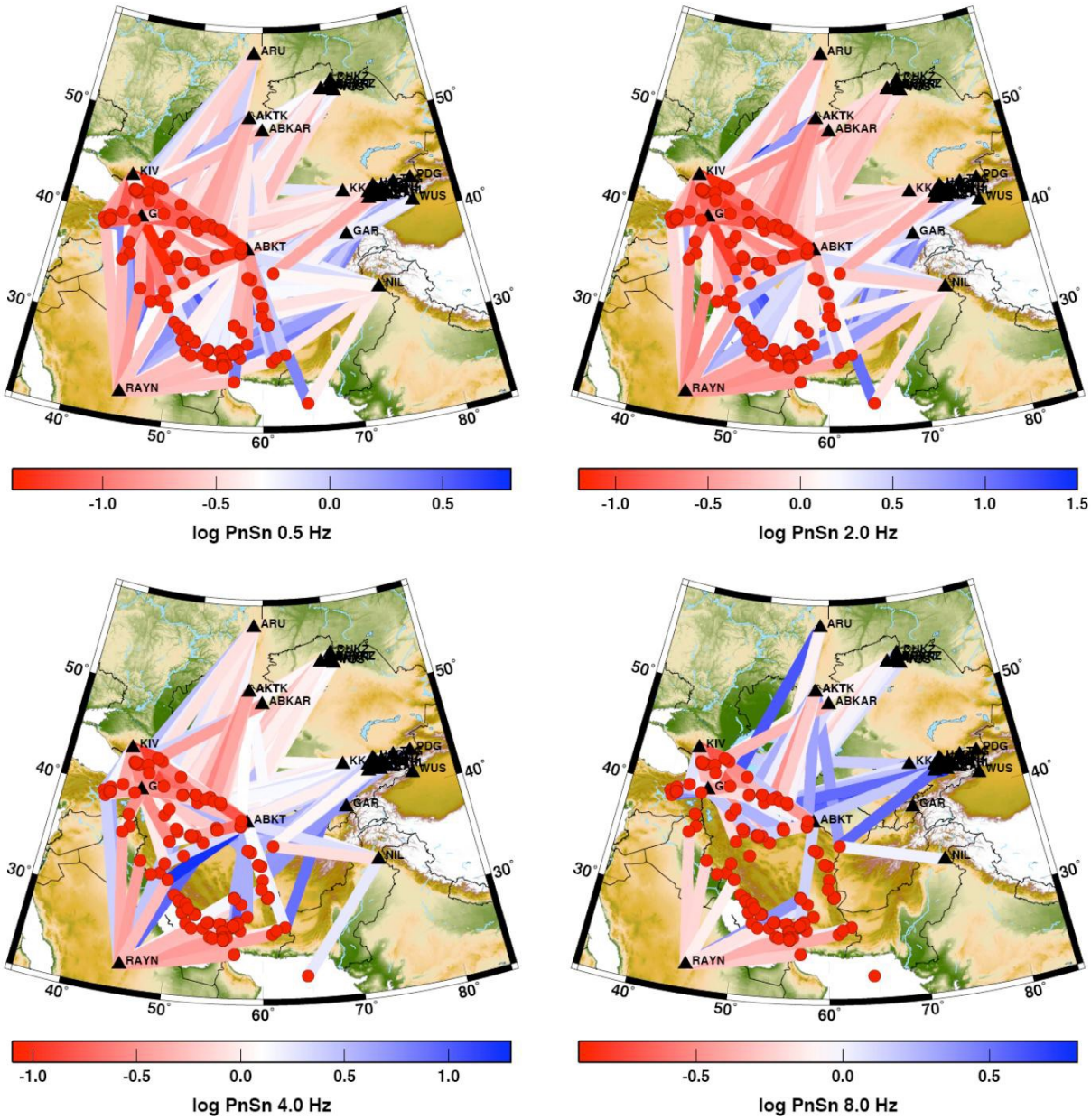

Figure 18. Similar to Figure 16, but for Pn/Sn.

In summary of initial analyses of IRIS data for this region, we are making excellent progress on calibrating source and distance effects for the Middle East, and assessing useful frequency ranges for regional seismic phases, particularly S waves.

3.2. Analysis of University of Tehran Data

Near the end of the first quarter, we did acquire some local/near-regional data recorded by Iranian stations for the same earthquakes considered in the previous section. Figure 19 shows examples of Lg/Pg spectral ratios. Figure 20 shows maps of Pg/Lg values at two frequencies for regional and local paths, indicating the distance dependence, path-specific variability, and bandwidth of local versus regional data. Bandwidth for GNI and ABKT (distances of about 600-730 km) for these earthquakes is limited to about 6-8 Hz. The local data have excellent SNR, even above 20 Hz.

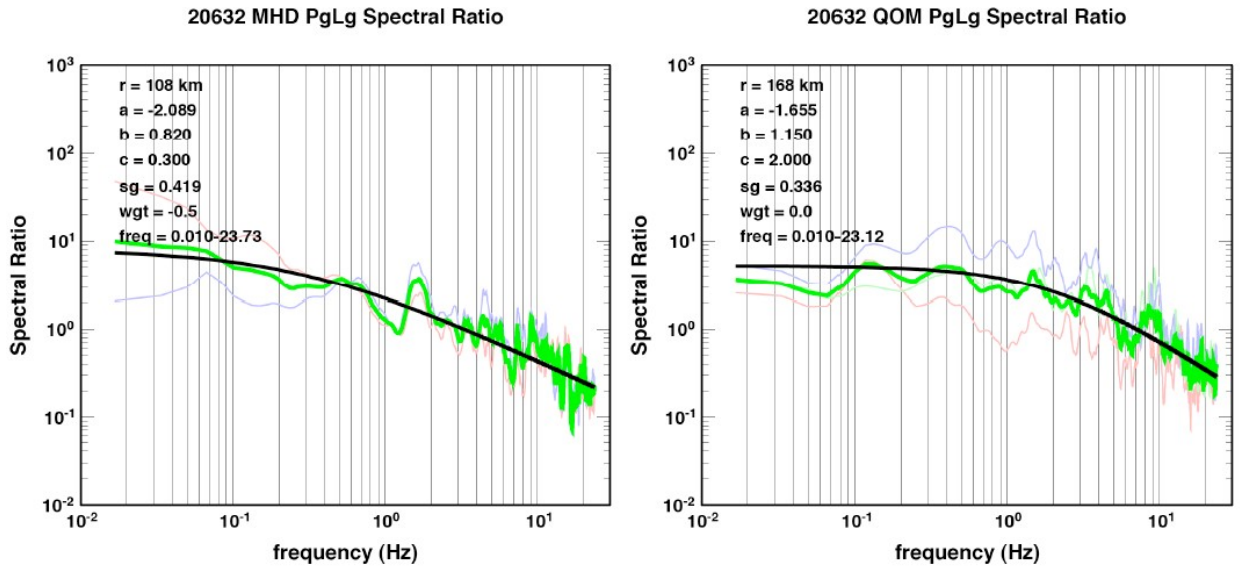

Figure 19. Examples of Lg/Pg spectra for an earthquake in northern Iran.

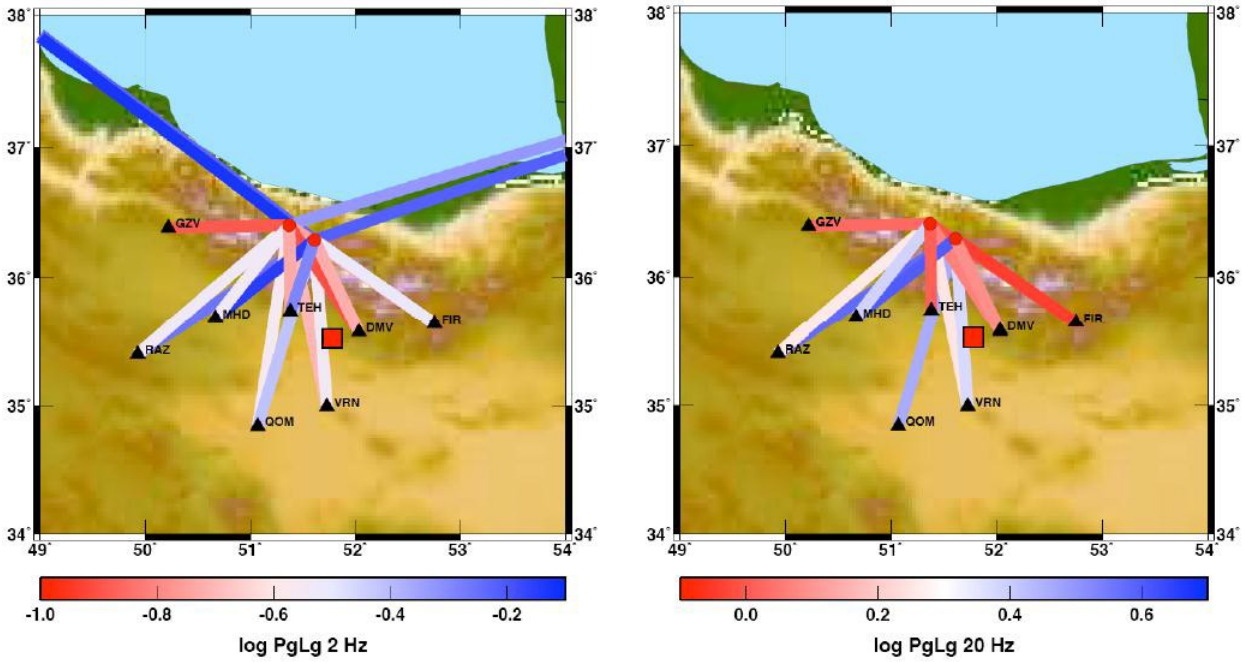

Figure 20. Pg/Lg values at 1 Hz (left) and 20 Hz (right) for regional and local paths from two events.

Large volumes of openly-available data from University of Tehran and International Institute of Earthquake Engineering and Seismology (IIEES) have already acquired by LANL and LLNL. Instrument responses are unavailable or unreliable for a significant fraction. In earlier analyses, we focused on earthquakes in southern Iran and one cluster (orid 20632) in northern Iran (see previous section). Here we focus on a larger set of earthquakes listed in the PDE for northern Iran (Figure 21). (Below, we also present our analysis of IIEES data.) One pair (orids 24640/24641), in particular, highlights the key issues and the benefits of our approach. Orid 24640 was an Mw 5.5 earthquake; orid 24641 was a subsequent (one day later) mb 4.1 event.

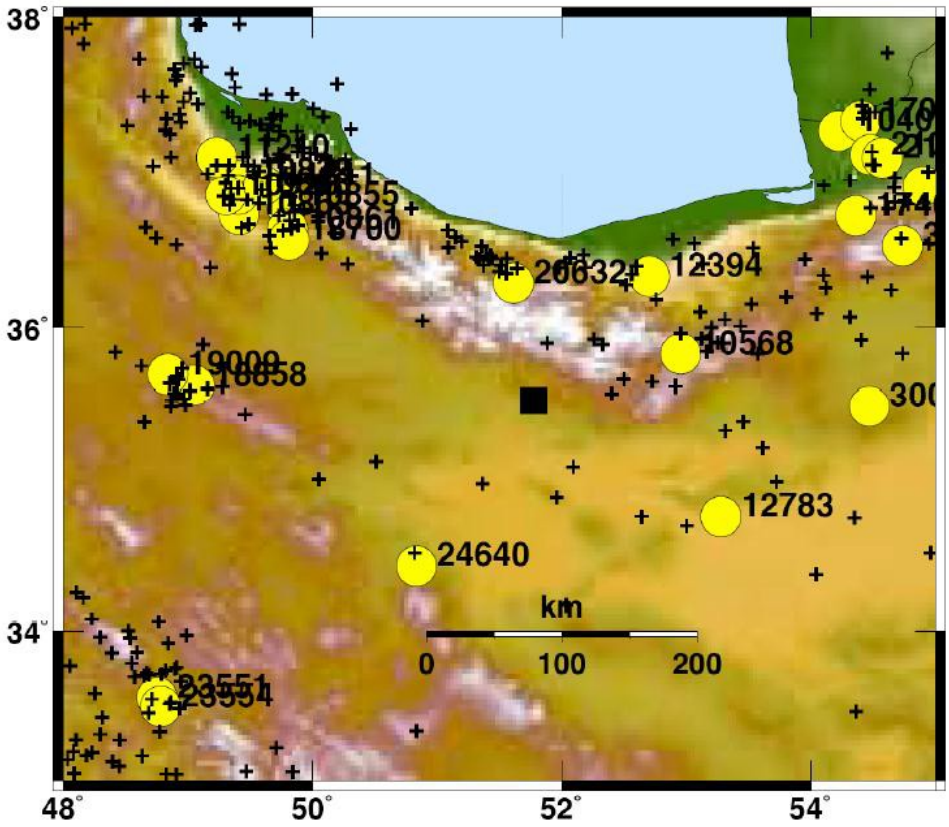

Figure 21. Map of events in northern Iran that are listed in the PDE. *Circles are mb≥5 earthquakes; "+" markers are smaller events. We acquired (Univ. of Tehran) data for these events.*

We have shown that IRIS data, using our EGF approach, gives good source estimates for many such pairs. Figure 22, however, shows unfiltered recordings for these two events at regional IRIS stations GNI, KIV, ABKAR, and KKAR. The mb 4.1 event clearly has inadequate SNR, except for marginal low-frequency Lg at GNI (top trace). An apparent Pn at KKAR (second to bottom trace) is actually an interfering local event. The recordings for the Mw 5.5 event exhibit very good signals, but note also the strong variability with distance and path. For example, the GNI recording shows much stronger Lg than Pn or Pg, but the KKAR recording (bottom trace) would seem to be very explosion-like (impulsive Pn and small S waves), in the absence of experience and calibration. This highlights the critical need to perform careful analysis for this region to prevent serious discrimination errors. This cannot be stressed too strongly: proper calibration of regional phases is essential for reliable interpretation of regional signals and discriminants.

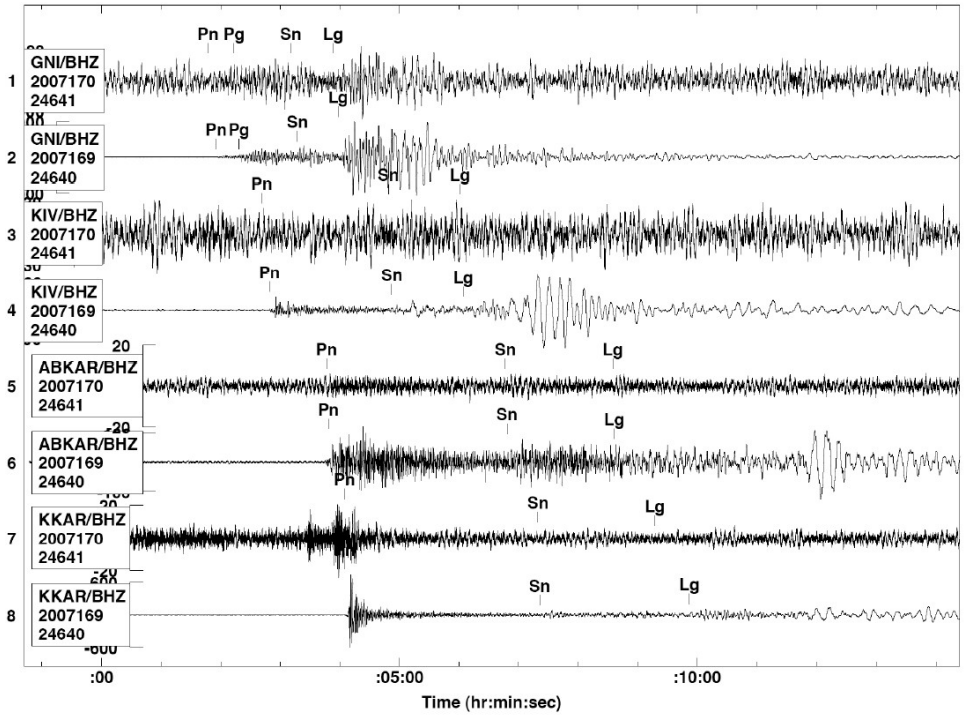

Figure 22. Regional IRIS recordings of an event pair in N. Iran. *The Mw 5.5 event has strong signals, but the mb 4.1 event lacks adequate SNR for EGF processing. A local event interferes with Pn at KKAR for the smaller event (second from bottom trace). Note the marked variability of the signals with distance and path.*

Figure 23 (left) shows the relative spectra at GNI (about 833 km away, the only adequate IRIS data) for this pair. Although the Mw and corner frequency estimates are not terrible (fortuitously), clearly the inadequate bandwidth of the mb 4.1 event at low and high frequencies makes these estimates very unstable/unreliable. These events were also recorded by 39 common in-country stations, ranging in epicentral distances of 103-811 km. Figure 23 (right) shows the relative spectra, using a subset of good data. Note that (1) we do not have responses for these data, but assume they did not change over the one-day interval between the events; (2) we use theoretical (IASP91) phase picks, which are early for Pn and Pg; and (3) the data for some stations or channels exhibit various glitches/clipping/problems that we have tried to exclude. Except for the Pn relative spectra (red curve, right plot of Figure 23), affected by early picks and lowest SNR, the various phases and coda give consistent Mw and corner frequency estimates. Given the source parameters, we use the strong signals for the larger event to estimate Q, spreading, and site effects for IRIS and other available stations with responses, as we illustrate for the path to ABKAR (stippled curve in).

Without reliable responses, the second use of in-country data that we proposed is to compute and fit P/S spectral ratios. As an example, Figure 24 shows the Lg/Pn spectral ratio for ABKAR, its fit, and comparisons to Q model predictions. The dotted curve, based on Pn and Lg Q results from amplitude tomography, differs greatly from the actual spectral ratio at frequencies relevant to discrimination, considerably over-predicting relative S-wave energy for this path. This would clearly lead to misidentification of earthquakes as explosions. Note also that the useful signal bandwidth, easily discernible in our analysis, is slightly higher than 3 Hz. Last, the Q predictions

from source-corrected spectra (stippled black), using the source parameter estimates from the right plot of Figure 23 (Univ. of Tehran data), is comparable to the direct fit of the Lg/Pn spectral ratio (solid black). Figure 25 shows an Lg/Pg spectral ratio at station BAF in Iran, 543 km from the event, exhibiting good bandwidth up to 16 Hz.

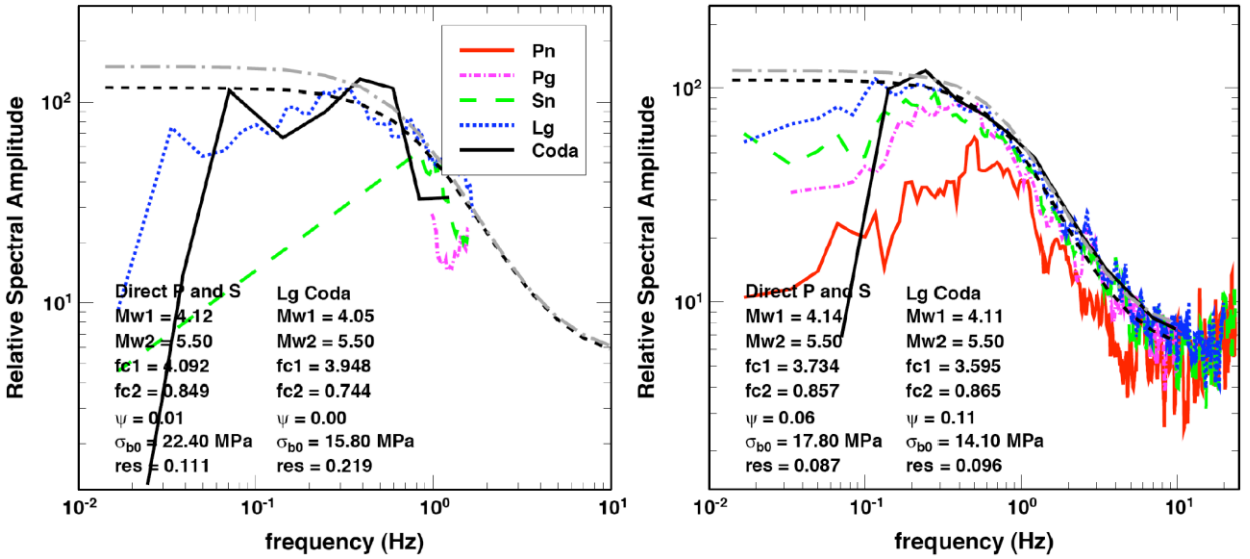

Figure 23. Relative spectra at the closest IRIS station, GNI (left), and using in-country network data (right). *Data at IRIS stations for the smaller event (orid 24641, mb 4.1) are inadequate to estimate reliable source parameters for the pair, while in-country data are sufficiently good.*

Figure 26 shows log Pg/Lg values at 4 Hz for the paths to 42 stations. These results, along with the source parameters, can be used to constrain multi-phase, multi-band amplitude tomography runs. Considering many events (e.g., Figure 21) and in-country stations, there is tremendous potential to accurately constrain tomography results for this area, providing reliable P/S discrimination results, where traditional tomography alone has significant errors (e.g., Figure 24).

Figure 27 shows the maximum frequencies of Pg/Lg for the larger (Mw 5.5, left plot) and smaller (Mw 4.1, right plot) events. The results indicate the useful frequency range of Lg for various distances/paths, showing clear trends with distance. One might expect that the much smaller event would have much lower maximum frequencies, but there is very little difference between the left and right plots. This is because the smaller event has a considerably higher corner frequency (and these are relatively high stress events), compensating for the smaller size. Thus, distance and Q seem to be the more significant drivers in determining useful frequency content than source size, at least for higher stress-drop events.

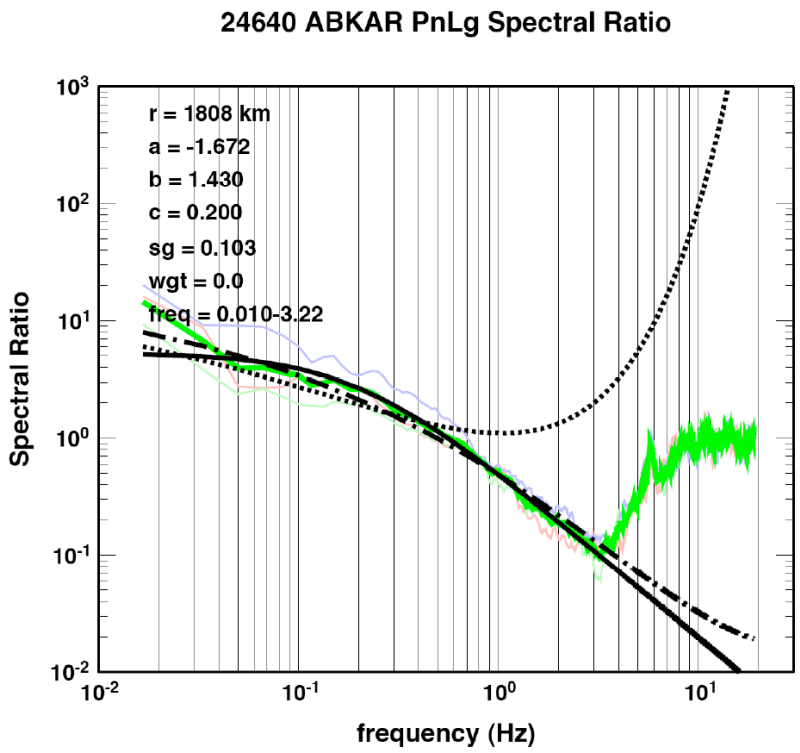

Figure 24. Lg/Pn spectral ratio, its fit (solid black), Q prediction from source-corrected spectra (stippled black), and from amplitude tomography (dotted black) for the path to station ABKAR.

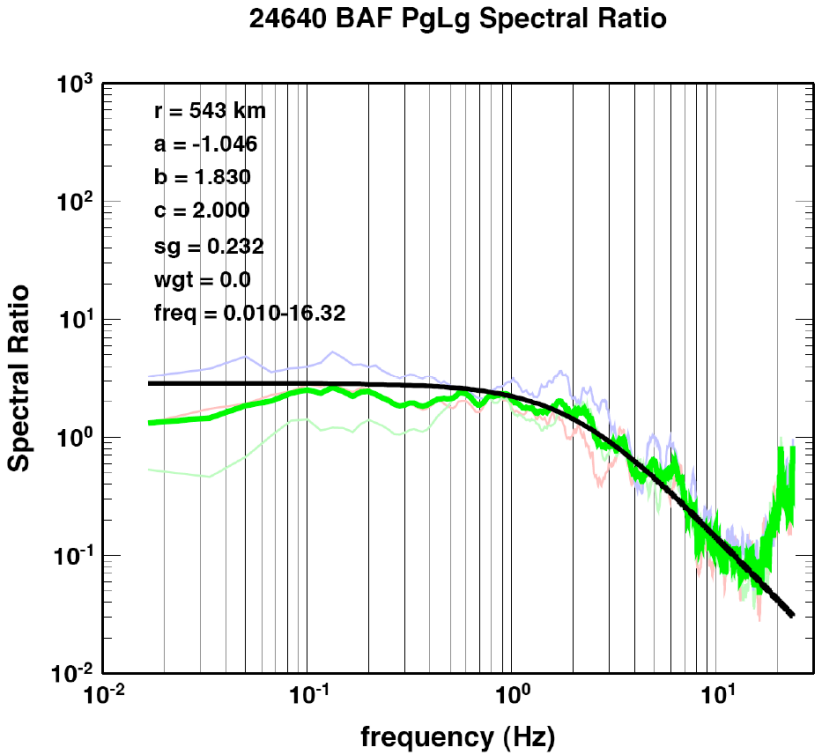

Figure 25. Lg/Pg spectral ratio and its fit (solid black) for the path to station BAF in Iran.

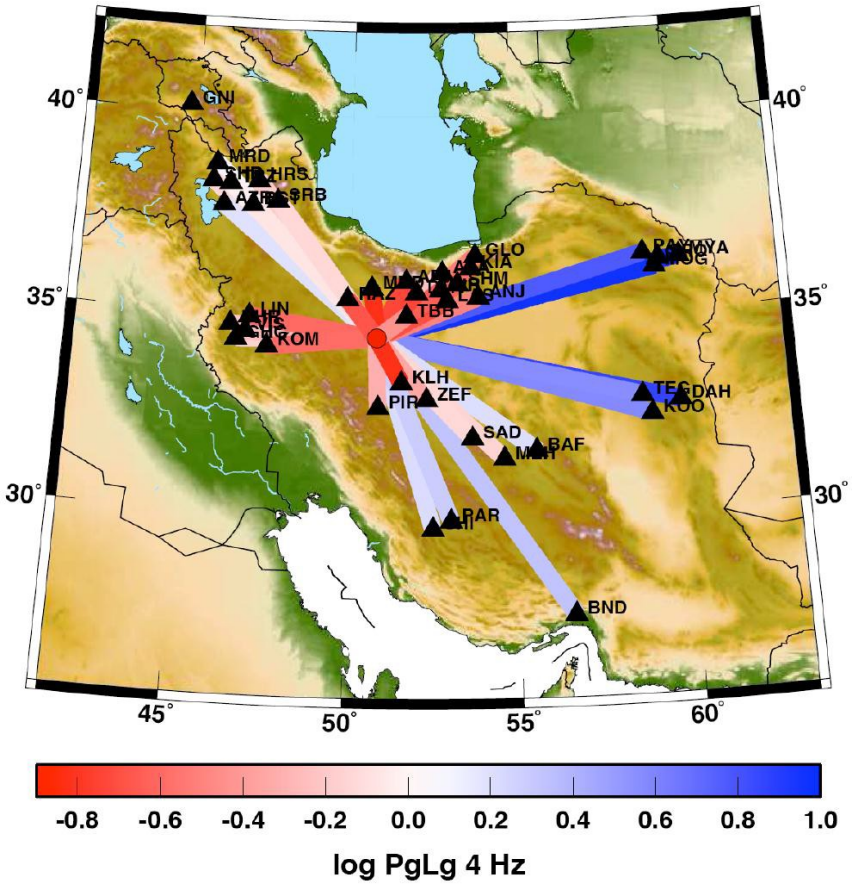

Figure 26. Pg/Lg values at 4 Hz for local and regional paths from the Mw 5.5 earthquake (orid 24640). *The results exhibit typical distance dependence, as well as path-specific variations.*

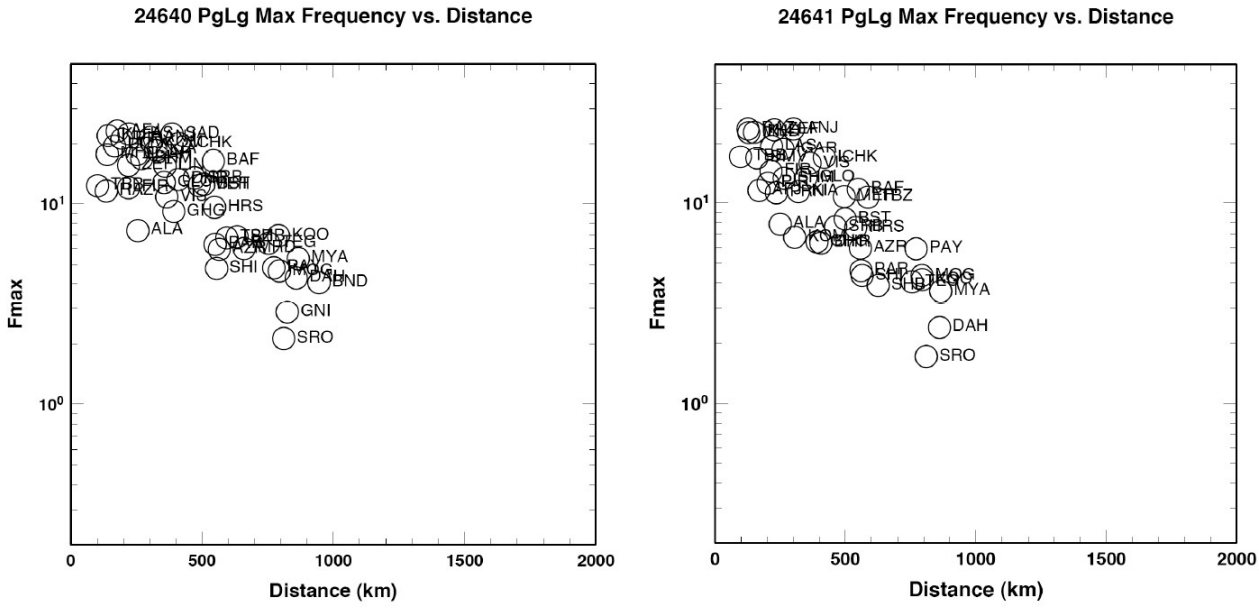

Figure 27. Maximum frequencies of Pg/Lg versus distance for the Mw 5.5 (left) and Mw 4.1 (right) events.

So given these results, we are forging ahead with processing this (Univ. of Tehran) data set. Figure 28 (left) shows a preliminary map of log Pg/Lg values at 1 Hz. These results have not yet been fully QC'd. Presently, this map is mainly intended to indicate the coverage and potential benefit for extensively characterizing signals of interest and path effects. For example, Figure 28 (right) shows the maximum frequency of Pg/Lg with good signal-to-noise for paths processed so far, to quantify bandwidth, particularly for S waves, for various paths and event sizes. At closer distances the maximum frequency is limited by the Nyquist frequency of 25 Hz. Most (particularly low) outliers are due to data quality problems. (Note that some events are outside the initial study area of Figure 21, simply because the database query was based on jdate, not orid. Thus, the events (red circles) are densest in the north, but there are some stragglers.) Once we QC these data, we will process event data for the entire country, which will fill in the region with a very dense set of paths. In reviewing the data, we have seen the following predominant types of problems affecting quality: (1) clock errors; (2) theoretical travel-time errors; and (3) bad data for one or more channels. All are straightforward to address, but simply take time and effort. As a ancillary benefit, we expect to provide clock corrections and manual phase picks back to LANL for their use. It is difficult currently to see patterns in the map of Figure 28, but there are clear spatial variations that need to be quantified and modeled.

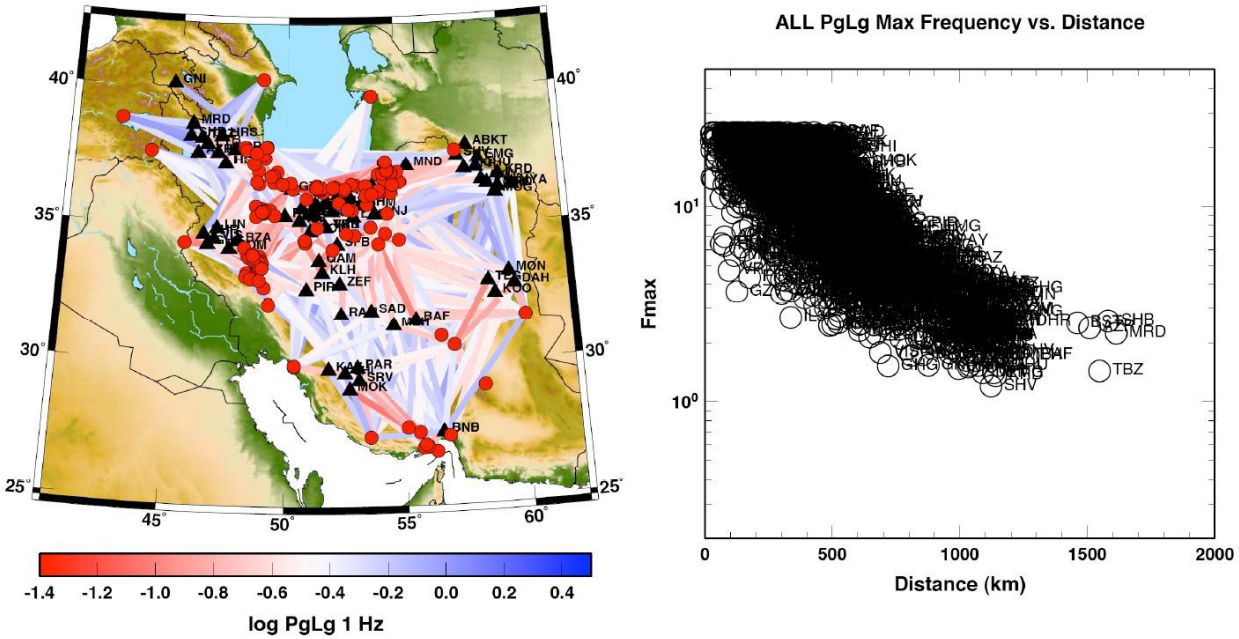

Figure 28. (left) Map of preliminary Pg/Lg values at 1 Hz for local and regional paths (Univ. of Tehran data) processed so far. (Right) Maximum frequencies of Pg/Lg versus distance for these paths; the scatter, which we plan to resolve, is due to variations in path-specific Q, source size, and some data quality issues.

3.3. Analysis of IIEES Data

Within the past month, we also assembled, made phase picks, and began analyzing IIEES data that Drs. Phillips and Richard Stead of LANL provided, including responses that are considered reliable for these stations. In fact, the overall quality of the IIEES data is generally superior to the Univ. of Tehran data. These events do not overlap with the events described above that are listed in the PDE. They include good spatial distribution and some nice aftershock sequences. Figure 29 represents IIEES data we are analyzing, including representative high-quality local and regional signals for an mb 5.3 earthquake. As mentioned before, this map indicates the excellent coverage of paths, but needs further analyses to characterize signals of interest. For example, similar to Figure 27, we have quantified the maximum frequency of Lg signals with good signal-to-noise for a subset of reviewed events.

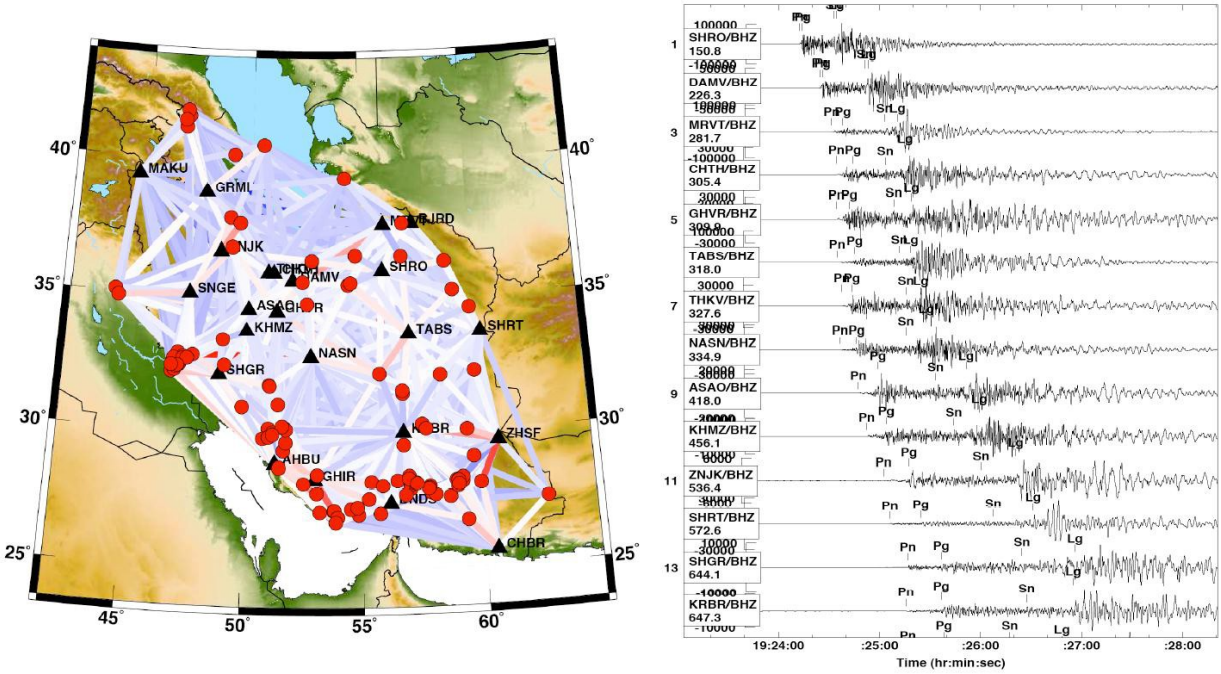

Figure 29. (Left) IIEES stations, events, and paths for which we are characterizing source and propagation effects. (Right) Examples of seismograms recorded at local and regional distances.

We have also processed and fit relative spectra for many of the pairs, to estimate source parameters, and then estimated Q for some of the corresponding paths (e.g., Figure 30). The Pn measurement windows and spectral variable require more work, as planned. We currently do not have tomography results for comparisons. However, Dr. Phillips confirms some of this qualitative Lg Q behavior in terms of geophysical structures (e.g., the Lut Block). Presently, we are making very good progress on several tasks. We plan to finish and present these results (source parameters and estimates of Q from source-corrected spectra) at the TIM.

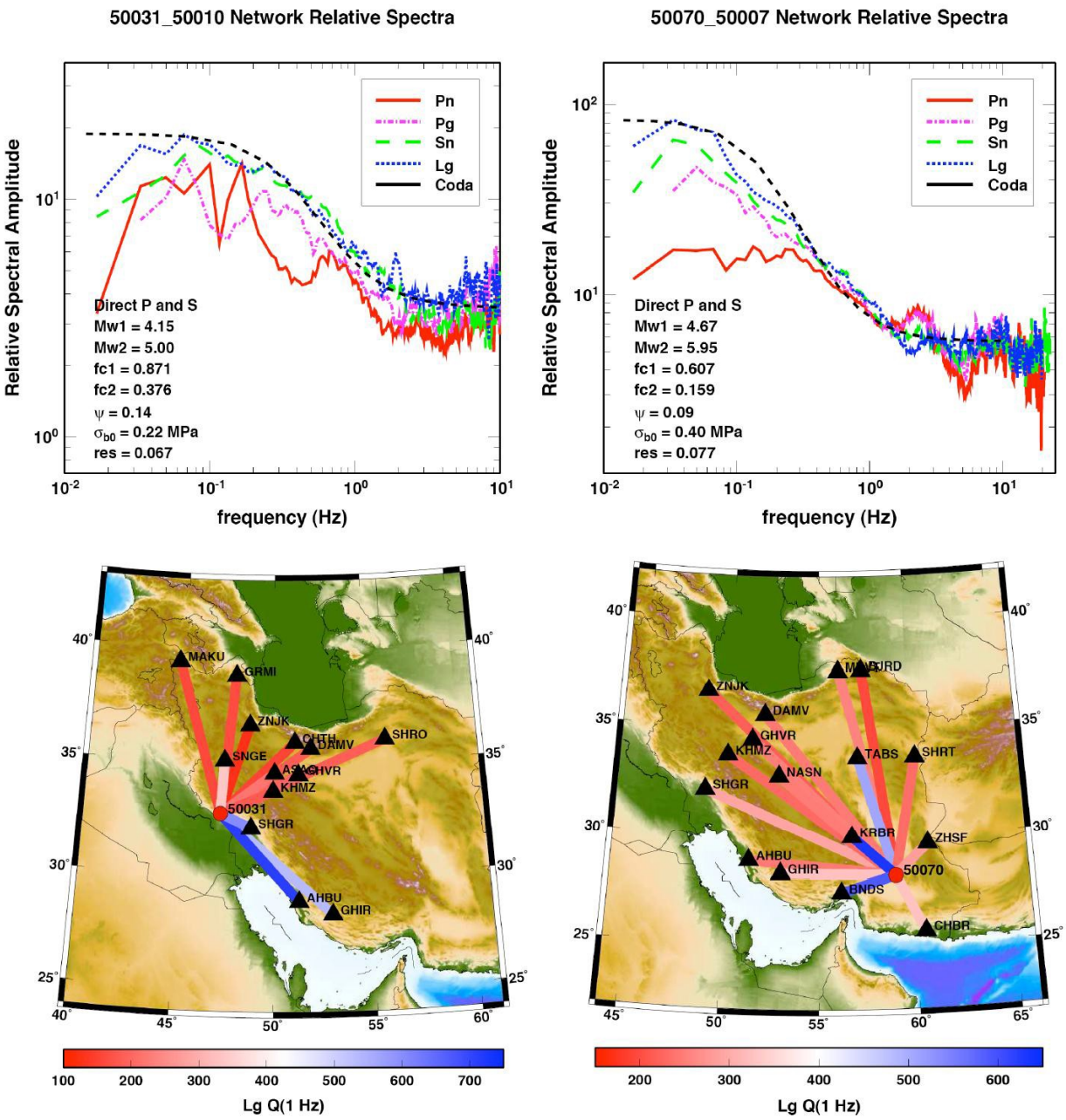

Figure 30. (Top plots) Relative spectra and source parameters for two of the clusters we have analyzed. (Bottom maps) Preliminary Lg Q_0 for paths corresponding to the upper source results.

4. CONCLUSIONS AND PLANS

Much of the work during this early stage of the project has been to assemble various data sets (openly available from IRIS, University of Tehran, and IIEES), make and refine theoretical phase picks, process spectra of regional phases, and perform various spectral fits, depending on the information (e.g., instrument responses) available. The spectral fits of source terms, Q, and P/S ratios are to be used to constrain amplitude tomography runs, which have unstable results (large errors) in this Middle East region. Based on our preliminary analysis, the results demonstrate the following (and, hence, the value of this effort):

1. IRIS data are sufficient to obtain source terms, corroborated by direct phases and coda, for some clusters, which can then be used to also estimate Q for various regional paths.
2. However, depending on the time period, station availability, location, and source size, IRIS data are insufficient to calibrate this region; in-country data can be used to estimate source and P/S effects in a manner that does not require reliable responses.
3. Relative P and S energy exhibits strong distance and path-specific variations (e.g., Figure 22) that must be properly calibrated to get meaningful/correct discrimination results.
4. As we have shown before, amplitude tomography results can have very large errors, leading to wrong discrimination results (e.g., Figure 24).
5. Using University of Tehran data, many good source terms (e.g, Figure 23, left) and P/S results (e.g., Figure 26) can be obtained and used to constrain tomography runs.
6. Most of the actual P/S spectral ratios do not have the curvature predicted by exponential attenuation functions. Rather, they are often fairly flat at low frequency and then decay like a power law of frequency, not an exponential of a frequency-dependent power law. A possible interpretation is that elastic scattering may be more responsible for differential frequency-dependent S/P behavior than anelastic attenuation represented by exponentially decaying terms, perhaps corroborating findings by Morozov (2008) and Morozov et al. (2008).
7. We determined the useful frequency ranges of P and S phases. The strongest dependence appears to be on distance and Q, particularly for high stress events. We have quantified such ranges for a wide range of events and paths. From this information, and accounting for Nyquist saturation issues, we can begin to quantify the maximum frequency as a function of magnitude, epicentral distance, and Q.
8. IIEES data have more reliable responses and fewer data quality problems than University of Tehran data, from which we are able to directly estimate source terms, as well as Q parameters for a dense set of paths.

We plan to continue processing the University of Tehran and IIEES data sets for earthquakes in the Middle East, focusing on the Iranian Plateau. Analyses include: (1) reviewing data quality, (2) fitting relative spectra to estimate source parameters, (3) fitting source-corrected spectra for IRIS and IIEES stations (with reliable responses); and (4) fitting various P/S ratios for stations without reliable responses. We plan to coordinate this effort with Drs. Phillips and Pasyanos, and participate in the Technical Interchange Meeting.

REFERENCES

Avants, M., T. Lay, X.-B. Xie, and X. Yang (2011), Effects of 2D random velocity heterogeneities in the mantle lid and Moho topography on Pn geometric spreading, *Bull. Seism. Soc. Am.,* **101**, pp. 126-140.

Bottone, S., M. D. Fisk, and G. D. McCartor (2002), Regional seismic event characterization using a Bayesian formulation of simple kriging, *Bull. Seism. Soc. Am.*, **92**, pp. 2277-2296.

Brune, J. N. (1970), Tectonic stress and the spectra of seismic shear waves from earthquakes, *J. Geophys. Res.,* **75**, pp. 4997-5009.

Fisk, M. D., H. L. Gray, and G. D. McCartor (1996), Regional discrimination without transporting thresholds, *Bull. Seism. Soc. Am.*, **86**, pp. 1545-1558.

Fisk, M. D. and W. S. Phillips (2013a), Constraining regional phase amplitude models for Eurasia. Part 1: accurate source terms and geometric spreading, *submitted to Bull. Seism. Soc. Am.*

Fisk, M. D. and W. S. Phillips (2013b), Constraining regional phase amplitude models for Eurasia. Part 2: frequency-dependent attenuation and site results, *submitted to Bull. Seism. Soc. Am.*

Fisk, M. D. and W. S. Phillips (2012), Constraining Source Terms, Regional Attenuation Models, Geometric Spreading, and Site Terms for Eurasia, AFRL-RV-PS-TR-2013- 0081, Alliant Techsystems, Newington, VA.

Fisk, M. D. and W. S. Phillips (2011), Constraining source terms, regional attenuation models, and site effects, *in Proceedings of the 2011 Monitoring Research Review: Ground-Based Nuclear Explosion Monitoring Technologies*, LA-UR-11-04823, Vol. 1, pp. 59-68.

Fisk, M. D. and W. S. Phillips (2009), A stepwise, iterative procedure to constrain stress drop, regional attenuation models, and site effects, *in Proceedings of the 2009 Monitoring Research Review: Ground-Based Nuclear Explosion Monitoring Technologies*, LA-UR-09-05276, Vol. 1, pp. 52-61.

Fisk, M. D. and S. R. Taylor (2006), Robust magnitude and path corrections for regional seismic phases in Eurasia by constrained inversion and enhanced kriging techniques, *in Proceedings of the 28th Monitoring Research Review, Ground-Based Nuclear Explosion Monitoring Technologies*, LA-UR-06-5471, Vol. 1, pp. 15-24.

Fisk, M. D., S. R. Taylor, W. R. Walter, and G. E. Randall (2010), Seismic Event Discrimination and Modeling Using Two-Dimensional Grids of Regional P/S Spectral Ratios, ATK-R-1744, Final Technical Report, NNSA Contract DE-AC52-07NA28116.

Morozov, I. B. (2008), PNE coda attenuation and scattering parameters in northern Eurasia, *in Proceedings of the 30th Monitoring Research Review, Ground-Based Nuclear Explosion Monitoring Technologies*, LA-UR-08-05261, Vol. 1, pp. 159-169.

Morozov, I. B., C. Zhang, J. N. Duenow, E. A. Morozova, and S. B. Smithson (2008), Frequency dependence of coda Q, Part 1: Numerical modeling and examples from Peaceful Nuclear Explosions, *Bull. Seism. Soc. Am.*, **98**, pp. 2615-2628.

Pasyanos, M. E., W. R. Walter, and E. M. Matzel (2009), A simultaneous multi-phase approach to determine P-wave and S-wave attenuation of the crust and upper mantle, *Bull. Seism. Soc. Amer.*, **99-6**, pp. 3314-3325, DOI: 10.1785/0120090061.

Sandvol, E., A. Kaviani, W. Ku, R. Gök, and G. Rumpker (2012), High-resolution regional phase attenuation models of the Iranian Plateau and Zagros, *in Proceedings of the 2012 Monitoring Research Review: Ground-Based Nuclear Explosion Monitoring Technologies*, LA-UR-12-24325, Vol 1, pp 95-104.

Sereno T. J., S. R. Bratt and T. C. Bache (1988), Simultaneous inversion of regional wave spectra for attenuation and seismic moment in Scandinavia, *J. Geophys. Res.*, **93**, pp. 2019-2035.

Street, R., R. Herrmann, and O. Nuttli (1975), Spectral charactristics of Lg wave generated by central United States earthquakes, Geophys. *J.R. Astron. Soc.*, **41**, pp.51-63

Taylor, S. R. and H. E. Hartse (1998), A procedure for estimation of source and propagation amplitude corrections for regional seismic discriminants, *J. Geophys. Res.*, **103**, pp. 2781-2789.

Walter, W. R., K. M. Mayeda, and H. J. Patton (1995), Phase and spectral ratio discrimination between NTS earthquakes and explosions. Part I: Empirical observations, *Bull. Seism. Soc. Am.*, **85**, pp. 1050-1067.

Yang, X. (2011), A Pn spreading model constrained with observed amplitudes in Asia, *Bull. Seism. Soc. Am.*, **101**,pp. 2201-2211.

Yang, X., T. Lay, X.-B. Xie, and M.S. Thorne (2007), Geometric spreading of Pn and Sn in a spherical Earth model, *Bull. Seism. Soc. Am.*, **97**, pp. 2053-2065.

LIST OF SYMBOLS, ABBREVIATIONS, AND ACRONYMS

AFRL	Air Force Research Laboratory
AFSPC	Air Force Space Command
AFWA	Air Force Weather Agency

DISTRIBUTION LIST

DTIC/OCP
8725 John J. Kingman Rd, Suite 0944
Ft Belvoir, VA 22060-6218 1 cy

AFRL/RVIL
Kirtland AFB, NM 87117-5776 2 cys

Official Record Copy
AFRL/RVBYE/Dr. Robert Raistrick 1 cy